Continuum Mech. Thermodyn. (2018) 30:233–266
https://doi.org/10.1007/s00161-017-0596-4

ORIGINAL ARTICLE

Felix A. Reich · Wilhelm Rickert · Wolfgang H. Müller

An investigation into electromagnetic force models: differences in global and local effects demonstrated by selected problems

Received: 2 June 2017 / Accepted: 2 September 2017 / Published online: 30 September 2017
© Springer-Verlag GmbH Germany 2017

Abstract This study investigates the implications of various electromagnetic force models in macroscopic situations. There is an ongoing academic discussion which model is "correct," *i.e.*, generally applicable. Often, *gedankenexperiments* with light waves or photons are used in order to motivate certain models. In this work, three problems with bodies at the macroscopic scale are used for computing theoretical model-dependent predictions. Two aspects are considered, total forces between bodies and local deformations. By comparing with experimental data, insight is gained regarding the applicability of the models. First, the total force between two cylindrical magnets is computed. Then a spherical magnetostriction problem is considered to show different deformation predictions. As a third example focusing on local deformations, a droplet of silicone oil in castor oil is considered, placed in a homogeneous electric field. By using experimental data, some conclusions are drawn and further work is motivated.

Keywords Electromagnetic force models · Total force · Local deformation · Experiments

Contents

Communicated by Andreas Öchsner.

F. A. Reich (✉) · W. Rickert · W. H. Müller
Institut für Mechanik, Kontinuumsmechanik und Materialtheorie, Technische Universität Berlin, Sek. MS. 2, Einsteinufer 5, 10587 Berlin, Germany
E-mail: felix.reich@tu-berlin.de

List of symbols

General quantities

$\boldsymbol{x}$	Position vector in current placement (m)
$\boldsymbol{X}$	Position vector in reference placement (m)
$\boldsymbol{v}$	Barycentric velocity (m/s)
$\boldsymbol{v}_I$	Barycentric surface velocity (m/s)
$\boldsymbol{w}$	Velocity of a singular surface (m/s)
$w_\perp$	Normal velocity of a singular surface (m/s)
$\boldsymbol{n}$	Normal vector (1)
P_n	nth LEGENDRE polynomial (1)
K	Complete elliptic integral of the first kind (1)
E	Complete elliptic integral of the second kind (1)
Π	Complete elliptic integral of the third kind (1)
B	Incomplete beta function (1)
${}_2\mathrm{F}_1$	A hypergeometric function (1)
R	Characteristic radius of a problem (m)
H	Characteristic length of a problem (m)
d	End-to-end distance between magnets (m)
κ	Normed end-to-end distance between magnets, $\kappa = d/R$ (1)
r	Radial spherical coordinate (m)
$\tilde{r}$	Dimensionless radial spherical coordinate, $\tilde{r} = r/R$ (1)
ϑ	Polar spherical angle, $\vartheta \in [0, \pi]$ (1)
x	Cosine of polar spherical angle (1)
ξ	Radial cylindrical coordinate (m)
$\tilde{\xi}$	Dimensionless radial cylindrical coordinate, $\tilde{\xi} = \xi/R$ (1)
z	Axial cylindrical coordinate [m]
$\tilde{z}$	Dimensionless axial cylindrical coordinate, $\tilde{z} = z/R$ (1)
φ	Azimuthal angle, $\varphi \in [0, 2\pi)$ (1)
V	Volume in current placement (m^3)
V_0	Volume in reference placement (m^3)
$\boldsymbol{u}$	Displacement field (m)
$\boldsymbol{u}_I$	Surface displacement field (m)
$\hat{u}$	Scale of surface displacement (m)
$\tilde{u}_\mathrm{P}$	Dimensionless pole displacement (1)
u_r	Radial displacement component w.r.t. $\boldsymbol{e}_r$ (m)
u_ϑ	Polar displacement component w.r.t. $\boldsymbol{e}_\vartheta$ (m)
$\boldsymbol{F}$	Deformation gradient $\boldsymbol{F} = \mathbf{1} + \boldsymbol{u} \otimes \nabla_X$ (1)
J	Determinant of deformation gradient (1)
$(\cdot)^\mathrm{I}$	Indicates interior domain of a problem
$(\cdot)^\mathrm{O}$	Indicates exterior domain of a problem
$\tilde{(\cdot)}$	A normalized dimensionless function (1)
$(\cdot)_I$	Interface quantity
$(\cdot)^\mathrm{S}$	Refers to silicone oil
$(\cdot)^\mathrm{C}$	Refers to castor oil
$\boldsymbol{e}_z$	Cylindrical axial unit vector (1)
$\boldsymbol{e}_\xi$	Cylindrical radial unit vector (1)
$\mathbf{1}$	Unit tensor of rank two (1)
$\mathbf{1}_I$	Interface projector, $\mathbf{1}_I = \mathbf{1} - \boldsymbol{n} \otimes \boldsymbol{n}$ (1)
∇	Nabla operator, (1/m)
∇_I	surface nabla, $\nabla_I = \mathbf{1}_I \cdot \nabla$ (1/m)

Continuum mechanics

$\boldsymbol{\sigma}$	CAUCHY stress tensor ($\mathrm{N/m^2}$)
p	Pressure ($\mathrm{N/m^2}$)

$\boldsymbol{\sigma}_I$	CAUCHY surface stress tensor ($\mathrm{N/m}$)
σ_I	Surface tension ($\mathrm{N/m}$)
$\boldsymbol{\varepsilon}$	Linear strain tensor (1)
$\boldsymbol{\varepsilon}_I$	Linear surface strain tensor (1)
m	Mass of a body (kg)
ρ	Mass density ($\mathrm{kg/m^3}$)
ρ_I	Surface mass density ($\mathrm{kg/m^2}$)
λ	LAMÉ's first parameter ($\mathrm{N/m^2}$)
μ	LAMÉ's second parameter ($\mathrm{N/m^2}$)
λ_I	First elastic surface parameter ($\mathrm{N/m}$)
μ_I	Second elastic surface parameter ($\mathrm{N/m}$)
ν	POISSON's ratio (1)
ψ	Gravitational potential ($\mathrm{m^2/s^2}$)
G	Gravitational constant $G = 6.67408 \star 10^{-11}\ \mathrm{m^3/(kg\,s^2)}$
$\boldsymbol{g}$	Gravitational specific force density ($\mathrm{m/s^2}$)
$\boldsymbol{F}^{\mathrm{tot.}}$	Total force acting on a body (N)
$\boldsymbol{f}$	Volumetric force density ($\mathrm{N/m^3}$)
$\boldsymbol{f}_I$	Surface force density ($\mathrm{N/m^2}$)
$\hat{f}$	Scale of surface force density ($\mathrm{N/m^2}$)
$\boldsymbol{q}$	Heat flux ($\mathrm{N/(m\,s)}$)
$\hat{r}$	Specific heating ($\mathrm{m^2/s^3}$)
u	Specific internal energy ($\mathrm{m^2/s^2}$)
χ_{v}	Compressibility factor (1)
e_{v}	Relative volume change (1)
γ	Pressure-related factor (1)

Electrodynamics

$\boldsymbol{B}$	Magnetic flux density (T)
$\boldsymbol{H}$	Potential of total electric current ($\mathrm{A/m}$)
$\boldsymbol{\mathfrak{H}}$	Potential of free electric current ($\mathrm{A/m}$)
$\boldsymbol{M}$	MINKOWSKI magnetization ($\mathrm{A/m}$)
$\boldsymbol{E}$	Electric field ($\mathrm{V/m}$)
$\boldsymbol{D}$	Potential of total electric charge ($\mathrm{C/m^2}$)
$\boldsymbol{\mathfrak{D}}$	Potential of free electric charge ($\mathrm{C/m^2}$)
$\boldsymbol{P}$	Polarization ($\mathrm{C/m^2}$)
V	Electric disturbance potential (V)
$\mathcal{V}$	Scaled electric disturbance potential (1)
$\boldsymbol{E}_0$	External electric field ($\mathrm{V/m}$)
$\boldsymbol{E}^{\mathrm{dist.}}$	Electric disturbance field ($\mathrm{V/m}$)
E_0	External electric field strength ($\mathrm{V/m}$)
M_0	Magnetization strength of a magnet ($\mathrm{A/m}$)
β	Direction factor of magnetization (1)
μ_0	Vacuum permeability ($\mathrm{N/A^2}$)
μ_{r}	Relative permeability (1)
ϵ_0	Vacuum permittivity $\mathrm{A^2s^2/(Nm^2)}$
ϵ_{r}	Relative permittivity (1)
q	Total electric charge density ($\mathrm{C/m^3}$)
q^{f}	Free electric charge density ($\mathrm{C/m^3}$)
q^{r}	Bound electric charge density ($\mathrm{C/m^3}$)
q_I^{f}	Singular free electric charge density ($\mathrm{C/m^2}$)
q_I^{r}	Singular bound electric charge density ($\mathrm{C/m^2}$)
$\boldsymbol{J}$	Total electric current density ($\mathrm{A/m^2}$)
$\boldsymbol{J}^{\mathrm{f}}$	Free electric current density ($\mathrm{A/m^2}$)
$\boldsymbol{J}^{\mathrm{r}}$	Bound electric current density ($\mathrm{A/m^2}$)

$\boldsymbol{J}_I$ Singular total electric current density ($\mathrm{A/m}$)
$\boldsymbol{J}_I^{\mathrm{f}}$ Singular free electric current density ($\mathrm{A/m}$)
$\boldsymbol{J}_I^{\mathrm{r}}$ Singular bound electric current density ($\mathrm{A/m}$)
$\boldsymbol{j}^{\mathrm{f}}$ Free diffusive electric current density ($\mathrm{A/m^2}$)
$\boldsymbol{j}_I^{\mathrm{f}}$ Singular free diffusive electric current density ($\mathrm{A/m}$)

Coupling of mechanics and electromagnetism

$\boldsymbol{\sigma}^{(\mathrm{EM})}$ Electromagnetic stress tensor ($\mathrm{N/m^2}$)
$\boldsymbol{g}^{(\mathrm{EM})}$ Electromagnetic momentum density ($\mathrm{N/m^2}$)
$\boldsymbol{f}^{(\mathrm{EM})}$ Electromagnetic volumetric force density ($\mathrm{N/m^3}$)
$\boldsymbol{f}_I^{(\mathrm{EM})}$ Electromagnetic surface force density ($\mathrm{N/m^2}$)
$(\cdot)^{\mathrm{L}}$ Quantity of generalized LORENTZ force model
$(\cdot)^{\mathrm{A}_i}$ Quantity of an ABRAHAM force model
$(\cdot)^{\mathrm{M}_i}$ Quantity of a MINKOWSKI force model
$(\cdot)^{\mathrm{EL}}$ Quantity of EINSTEIN–LAUB force model

In problems of multiphysics, symbols often carry multiple meanings. For example, the letter μ refers to LAMÉ's second elastic parameter in elasticity and to magnetic permeability in electromagnetism. In order to avoid confusions regarding the meaning of the symbols in this work, we list all symbols together with their corresponding meaning and SI unit.

1 Introduction

The goal of this paper is to give insight into the force coupling of mechanics and electromagnetism by analyzing selected problems. In literature, there are many suggestions which model of the electromagnetic force is "correct." Hopefully a model can be found, which holds for arbitrary matter and dynamical contexts. However, the existence of such a model is by no means guaranteed. In the ongoing discussion in academia, many *gedankenexperiments* are used in order to push certain models. These are often based upon the dynamics of light waves or considerations of photons.

It is the believe of the authors of this work that *real* experiments can give insight into the applicability of the individual force models. Such experiments should be conducted on bodies of finite size, which can be modeled by using continuum physics. When considering bodies at the macroscopic scale, every electromagnetic force model implies

– an acting *total* force and
– distributions of *local* force densities.

This is an important issue, as for example, two models may yield the same total force but different local forces. In continuum mechanics it is clear that even if two loadings yield the same total force on a body, the deformation may vary considerably, depending on the distribution of the load. Therefore, measurement of total forces *and* of the deformations may give insight to the applicability of a force model. It is probably not possible to prove mathematically that a certain force model is "correct." However, by conducting many experiments with different matter and loading scenarios, it should be possible to reduce the number of force models. Hopefully, this way a most generally applicable force model can be found. In this sense, we consider an electromagnetic force model to be "correct," if its predictions of the total force that acts on a body as well as of the distribution of the local force agree with experiments. In contrast to total forces acting on bodies, distributions of force cannot be measured directly. However, their implications can be measured, *e.g.*, displacement figures are observable. For example, it is possible that various electromagnetic force models yield the same prediction of total force, even though they imply different displacement fields. In this paper, these differences are demonstrated with a few selected force models in context of some static problems.

The underlying assumption of all electromagnetic force models is that mechanical linear momentum is not a conserved quantity. The electromagnetic force is considered a production quantity. For example, neither kinetic energy nor internal energy is a conserved quantity. However, the sum of both energies is conserved as the production terms in form of the inner friction cancel out. This motivates the assumption that there exists a balance of linear electromagnetic momentum. The sum of this balance with the (classical) mechanical

momentum balance should not possess a production term, *i.e.*, the electromagnetic force will cancel out. The "proper" form of the electromagnetic momentum balance introduces a density of electromagnetic momentum, an electromagnetic stress tensor and the electromagnetic force density. It will be shown that the form of the local equation within a body also implies the form of the electromagnetic force on interfaces.

From the point of view of continuum physics, it is known that the interfaces between bodies must be treated with special care. Here fields may possess high gradients that cannot be resolved on the continuum scale. Therefore, at such surfaces, fields are modeled as discontinuities. Depending on the materials in contact, there may be distributed mass, stress, etc. on such an interface. This implies that there are additional local balance equations for interfaces. Consideration of these equations and of the interface form for every electromagnetic model-dependent force is important in the analysis. This will be detailed in this work.

There are many electromagnetic force models in the literature. Hence, for conciseness, only a few selected ones are introduced and exemplified in this chapter. In this paper, these models are not derived and also not discussed in detail (from a theoretical point of view)—there are many investigations of the various theories, *e.g.*, [16]. Here, the used models are only stated briefly and their implications are investigated. In order to gain insight into the applicability of the various considered force models, the following static problems are considered:

1. The total force between two coaxial equal cylindrical magnets will be computed with the considered models. Depending on the direction of the magnetization of the magnets, they can either attract or repel each other. By using the various models, the total force will be computed. The results are compared with conducted experiments using a microtensile testing machine.
2. As an example for local effects, an elastic and homogeneously magnetized sphere is considered. The magnetic self-field interacts with the magnetization, allowing for a model-dependent prediction of electromagnetic forces. These cause magnetostriction of the sphere, which can be computed for small strains by using the method of HIRAMATSU and OKA. With different force models employed, varying deformation figures will result. However, no experimental data are currently available for this problem. The results may motivate future experiments in this field, either for this or for a similar problem.
3. A second example is considered to show local effects of the models. A (spherical) drop of silicone oil is submerged in castor oil, and the setup is placed in a homogeneous electric field. Due to the different permittivities of the oils, a (model-dependent) deformation is to be expected. On the interface between the oils there exists a surface stress. This stress is modeled here for small displacements. The resulting field equations on the interface are solved for the surface displacement. Since this experiment was previously reported in the literature, the computed displacements can be compared with experimental photographs.

By investigating all aforementioned problems, the applicability of the considered force models can be analyzed. As these are static problems, this classical three-dimensional mechanical momentum equation (that is EUCLIDean invariant) can be used in the analysis.

This paper starts with a *gedankenexperiment* on gravitation. It serves well to show a fundamental difficulty in the formulation of electromagnetic force models, where there is certain freedom in the relation between the electromagnetic volume and surface force densities. In the next section, the general coupling of continuum mechanics and electromagnetism is introduced and discussed, independent of a force model. Here, the relation between volume and surface force is detailed. Next, a few selected electromagnetic force models are introduced, and the individual momentum densities, stress measures, and force densities are shown. In the subsequent three sections, the aforementioned problems are mathematically examined and, with the exception of the magnetostriction problem, compared to experimental data. Last, the findings are summarized and discussed.

2 A *gedankenexperiment* with gravitation

To become familiar with the problems that are related to electromagnetic force models, let us re-investigate NEWTON's law of gravitation:

$$\Delta\psi(\boldsymbol{x}) = 4\pi G\rho(\boldsymbol{x}), \quad \boldsymbol{g}(\boldsymbol{x}) = -\nabla\psi(\boldsymbol{x}).$$

Let us now investigate a body without any external influences, *e.g.*, a body in empty space (say). Here, the total force of the body reads

$$\boldsymbol{F}^{\text{tot.}} = \int_{\Omega} \boldsymbol{f}\,\mathrm{d}V, \quad \boldsymbol{f} = \rho\boldsymbol{g}.$$

Of course without any external influences, this force vanishes. However, for the sake of the argument, let us not assume so *a priori*. As a special case, we consider a homogeneous and constant mass density, $\rho = \rho_0$. Then, one can write via GAUSS' law

$$\boldsymbol{F}^{\text{tot.}} = \int_{\Omega} \boldsymbol{f}\,\mathrm{d}V = -\int_{\Omega} \rho_0 \nabla\psi\,\mathrm{d}V = -\oint_{\partial\Omega} \rho_0 \psi \boldsymbol{n}\,\mathrm{d}A. \tag{2.1}$$

Even though this reformulation is mathematically correct, it can be exploited to state an (absurd) gravitational force model. Define a surface force density

$$\boldsymbol{f}_I = -\rho_0 \psi \boldsymbol{n}$$

and claim that this is the "true" density of force; hence there is no volumetric force density. Obviously, the global force is the same, *i.e.*, zero. However, different local effects can be observed. As an example, let us analyze an isotropic linear-elastic sphere of radius R with these two gravitational force models. First, the POISSON equation for ψ readily yields

$$\psi(\boldsymbol{x}) = \tfrac{2}{3}\pi G\rho_0(r^2 - 3R^2)$$

in the interior, unique up to a constant. With the mass of the sphere, $m = {}^{4\pi}/_{3} R^3\rho_0$, the force densities of the two models are

$$\boldsymbol{f} = -\rho_0 \frac{mG}{R^3} r\boldsymbol{e}_r, \quad \text{or} \quad \boldsymbol{f}_I = \frac{mG\rho_0}{R}\boldsymbol{e}_r.$$

Employing HOOKE's law of linear elasticity,

$$\boldsymbol{\sigma} = \lambda \mathrm{tr}(\boldsymbol{\varepsilon})\mathbf{1} + 2\mu\boldsymbol{\varepsilon}, \quad \boldsymbol{\varepsilon} = \tfrac{1}{2}(\nabla \otimes \boldsymbol{u} + \boldsymbol{u} \otimes \nabla),$$

the first model implies for the equilibrium

$$\nabla \cdot \boldsymbol{\sigma} = -\boldsymbol{f}, \qquad (\boldsymbol{e}_r \cdot \boldsymbol{\sigma})_{r=R} = \mathbf{0}, \tag{G1}$$

where $\boldsymbol{u}$ is the displacement and $\boldsymbol{\sigma}$ the CAUCHY stress tensor. The second model yields

$$\nabla \cdot \boldsymbol{\sigma} = \mathbf{0}, \qquad (\boldsymbol{e}_r \cdot \boldsymbol{\sigma})_{r=R} = \boldsymbol{f}_I, \tag{G2}$$

using the same stress measure. Of course, the displacements are unique only up to rigid body modifications. Due to spherical symmetry, $\boldsymbol{u} = u_r(r)\boldsymbol{e}_r$, these problems are readily solved. With $\tilde{r} = {}^{r}/_{R}$ there follows

$$\boldsymbol{u}^{(1)} = \frac{\rho_0 mG}{\mu}\tilde{r}\frac{(2+3\frac{\lambda}{\mu})\tilde{r}^2 - 6 - 5\frac{\lambda}{\mu}}{10(2+\frac{\lambda}{\mu})(2+3\frac{\lambda}{\mu})}\boldsymbol{e}_r, \qquad \boldsymbol{u}^{(2)} = \frac{\rho_0 mG}{\mu}\frac{\tilde{r}}{2+3\frac{\lambda}{\mu}}\boldsymbol{e}_r.$$

The radial displacements are normalized by $u_r = \rho_0 mG\mu^{-1}\tilde{u}_r$ and visualized in Fig. 1. Clearly, the results are very different from one another, even though both models yield a vanishing *total* force acting on the sphere. The *local* forces and, consequently, the displacements are not equal. What went wrong here? In the context of Eq. (2.1), the localization theorem was violated, and therefore, any subsequent analysis is invalid.

Why did we consider this example? It can be seen that different distributions of volume and surface forces lead to differently deformed objects, even if the total force acting on the body is equal. With electromagnetic force models, there are certain degrees of freedom w.r.t. volume and surface forces. In contrast to the example considered here, it is not intuitively clear which model is physically correct. This will subsequently be discussed.

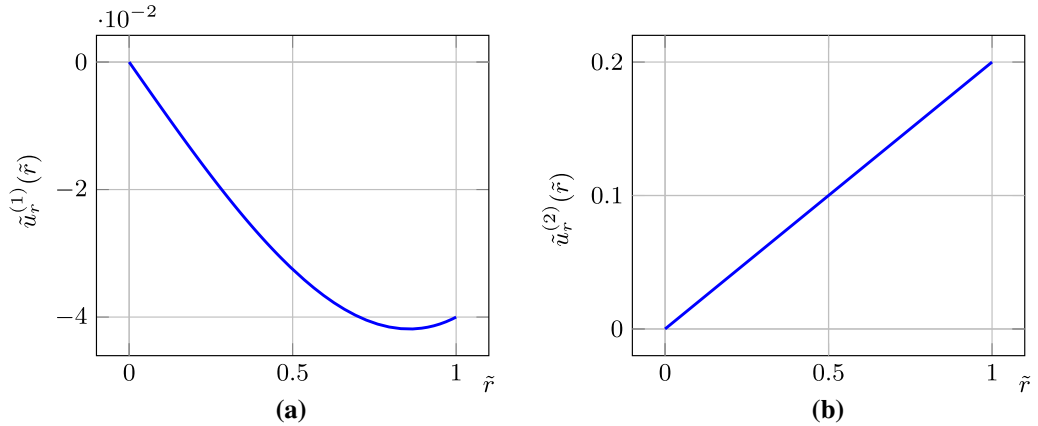

Fig. 1 Normed radial displacements of both gravitational models. For visualization, the ratio $\lambda/\mu = 1$ was employed. **a** NEWTON's gravitation. **b** Absurd gravitation model

3 Coupling of mechanics and electrodynamics

In continuum mechanics, additive quantities are balanced. In balances of conserved quantities, there may be supply terms (that can be deactivated, in theory) but no so-called production terms. A production term models some kind of reaction that cannot be controlled directly. Let us consider the classical balance of kinetic energy (without any electromagnetic influences)

$$\rho \frac{\mathrm{d}}{\mathrm{d}t}\left(\frac{\boldsymbol{v}\cdot\boldsymbol{v}}{2}\right) - \nabla\cdot(\boldsymbol{v}\cdot\boldsymbol{\sigma}) = -(\boldsymbol{v}\otimes\nabla)\cdot\cdot\,\boldsymbol{\sigma} + \boldsymbol{v}\cdot\rho\boldsymbol{f}.$$

In this equation, $\boldsymbol{\sigma}$ is the (CAUCHY) stress tensor, ρ the density of mass, $\boldsymbol{v}$ the barycentric velocity, and $\boldsymbol{f}$ is the specific volume force. The double contraction $(\cdot\cdot)$ of two tensors of rank two is given by $\boldsymbol{A}\cdot\cdot\,\boldsymbol{B} = A_{ij}B_{ij}$, if the components are given in an orthonormal basis. The specific body force is due to long range (gravitational) effects. In theory, if a body is moved far away from other masses, it is possible to deactivate this term. Hence, $\boldsymbol{v}\cdot\rho\boldsymbol{f}$ can be interpreted as a supply term of kinetic energy. However, $\boldsymbol{\sigma}$ models short-range effects and can therefore not be deactivated directly, and hence $-(\boldsymbol{v}\otimes\nabla)\cdot\cdot\,\boldsymbol{\sigma}$ is a production term. This production is called internal friction. Therefore, kinetic energy is not conserved. However, there is also a balance of internal energy. Without electromagnetic influences, it reads

$$\rho\frac{\mathrm{d}u}{\mathrm{d}t} + \nabla\cdot\boldsymbol{q} = (\boldsymbol{v}\otimes\nabla)\cdot\cdot\,\boldsymbol{\sigma} + \rho\hat{r},$$

where u is the specific density of internal energy, $\boldsymbol{q}$ is the heat flux, and $\hat{r}$ a specific radiation density. It is commonly assumed that $\hat{r}$ can be controlled. Adding these balances yields

$$\rho\frac{\mathrm{d}}{\mathrm{d}t}\left(\frac{\boldsymbol{v}\cdot\boldsymbol{v}}{2}+u\right) + \nabla\cdot(-\boldsymbol{v}\cdot\boldsymbol{\sigma}+\boldsymbol{q}) = \boldsymbol{v}\cdot\rho\boldsymbol{f} + \rho\hat{r},$$

and there is no production term anymore. This is the local balance of total energy, a conserved quantity. Let us now consider the balance of linear momentum with electromagnetic influences

$$\rho\frac{\mathrm{d}\boldsymbol{v}}{\mathrm{d}t} - \nabla\cdot\boldsymbol{\sigma} = \rho\boldsymbol{f} + \boldsymbol{f}^{(\mathrm{EM})} \quad\Leftrightarrow\quad \frac{\partial}{\partial t}(\rho\boldsymbol{v}) + \nabla\cdot(\rho\boldsymbol{v}\otimes\boldsymbol{v}-\boldsymbol{\sigma}) = \rho\boldsymbol{f} + \boldsymbol{f}^{(\mathrm{EM})},$$

where $\boldsymbol{f}^{(\mathrm{EM})}$ is a force density due to electromagnetic field. This density can also not be directly controlled and must therefore be considered as a production term. Linear (mechanical) momentum in not a conserved quantity from this viewpoint. As in the case of the energy balances, one suspects that there exists a total momentum balance without any production term to model some kind of conserved yet undefined total momentum. Therefore, another balance should exist of the form

$$\frac{\partial}{\partial t}(\boldsymbol{g}^{(\mathrm{EM})}) - \nabla\cdot\boldsymbol{\sigma}^{(\mathrm{EM})} = -\boldsymbol{f}^{(\mathrm{EM})}, \tag{3.1}$$

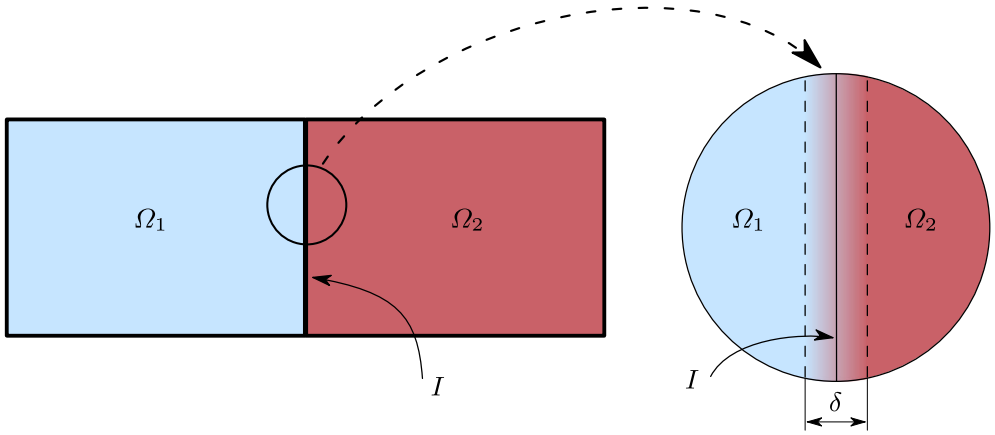

Fig. 2 Transition zone between two regular domains. High gradients may exist in a small transition zone that cannot be resolved on a macroscopic scale. The situation is handled in an idealized manner by using discontinuous functions w.r.t. the "singular" surface I. The transition zone Ω_δ is determined by I and a characteristic width δ

so that

$$\frac{\partial}{\partial t}(\rho \boldsymbol{v} + \boldsymbol{g}^{(\mathrm{EM})}) + \nabla \cdot (\rho \boldsymbol{v} \otimes \boldsymbol{v} - \boldsymbol{\sigma} - \boldsymbol{\sigma}^{(\mathrm{EM})}) = \rho \boldsymbol{f}$$

is a balance of a conserved momentum quantity. Regretfully, the densities and the flux (and even the force on the right-hand side) in the balance (3.1) are not known in general. The flux $\boldsymbol{\sigma}^{(\mathrm{EM})}$ is commonly referred to as electromagnetic stress tensor. There is a vast number of possible candidates resulting in many ongoing academic disputes. This point will be discussed in detail in the next section.

Note that Eq. (3.1) already determines the structure of the surface force. For a small volumetric region containing the boundary of a body, one can define the surface force density for the region considered in Fig. 2. The considered volume Ω_δ has two large plane surfaces parallel to the boundary of the original bodies. The distance between the two planes is given by a smallness parameter δ. By shrinking δ, the connecting side surfaces of Ω_δ tend to zero, and the volume degenerates to the mid-sectional plane I. By making use of this idea, a surface force w.r.t. the plane I can be defined through

$$\begin{aligned}
\int_I \boldsymbol{f}_I^{(\mathrm{EM})}\,\mathrm{d}A &:= \lim_{\delta \searrow 0} \int_{\Omega_\delta} \boldsymbol{f}^{(\mathrm{EM})}\,\mathrm{d}V = \lim_{\delta \searrow 0} \int_{\Omega_\delta} \left(-\frac{\partial \boldsymbol{g}^{(\mathrm{EM})}}{\partial t} + \nabla \cdot \boldsymbol{\sigma}^{(\mathrm{EM})} \right) \mathrm{d}V \\
&= -\lim_{\delta \searrow 0} \frac{\mathrm{d}}{\mathrm{d}t} \int_{\Omega_\delta} \boldsymbol{g}^{(\mathrm{EM})}\,\mathrm{d}V + \lim_{\delta \searrow 0} \oint_{\partial \Omega_\delta} \boldsymbol{n} \cdot (\boldsymbol{w} \otimes \boldsymbol{g}^{(\mathrm{EM})} + \boldsymbol{\sigma}^{(\mathrm{EM})})\,\mathrm{d}A \\
&= \int_{A_{\mathrm{left}}} \boldsymbol{n} \cdot (\boldsymbol{w} \otimes \boldsymbol{g}^{(\mathrm{EM})} + \boldsymbol{\sigma}^{(\mathrm{EM})})\,\mathrm{d}A + \int_{A_{\mathrm{right}}} \boldsymbol{n} \cdot (\boldsymbol{w} \otimes \boldsymbol{g}^{(\mathrm{EM})} + \boldsymbol{\sigma}^{(\mathrm{EM})})\,\mathrm{d}A \\
&= \int_I \boldsymbol{n} \cdot [\![\boldsymbol{w} \otimes \boldsymbol{g}^{(\mathrm{EM})} + \boldsymbol{\sigma}^{(\mathrm{EM})}]\!]\,\mathrm{d}A.
\end{aligned}$$

In the calculation, REYNOLDS' transport theorem and GAUSS' theorem were employed. This analysis holds for an arbitrary surface region, and we find that

$$\boldsymbol{f}_I^{(\mathrm{EM})} = \boldsymbol{n} \cdot [\![\boldsymbol{w} \otimes \boldsymbol{g}^{(\mathrm{EM})} + \boldsymbol{\sigma}^{(\mathrm{EM})}]\!] \qquad \forall \boldsymbol{x} \in \partial\Omega. \tag{3.2}$$

For a definition of the jump brackets $[\![\cdot]\!]$ and also of the mean value brackets $\langle\cdot\rangle$, see Eqs. (A.1).

It can be noted that there are other approaches to model the electromagnetic interaction. For example, KOVETZ proposed in [18] an entropy-based procedure to model the interaction in a material-dependent manner. In the presented procedure, he postulated the form of an extended energy flux. Recently, [35] examined these postulates and derived KOVETZ' equations, *e.g.*, the non-standard form of the CLAUSIUS–DUHEM inequality. This derivation is based on first principles of continuum mechanics and electromagnetism. Therein, the forms

of the electromagnetic force as well as of the power are assumed *a priori*. There is another interesting point raised in [35] in context of domains where all electromagnetic fields are sufficiently smooth. In those regions, there is no surface force, *i.e.*, the total electromagnetic force is then given by $\boldsymbol{F} = \int_\Omega \boldsymbol{f}^{(\mathrm{EM})}\,\mathrm{d}V$. If in this case the total force agrees with measurements, one can argue that $\boldsymbol{f}^{(\mathrm{EM})}$ is the correct local distribution of force due to the localization theorem. However, in most technical applications, there are singular surfaces, *e.g.*, the surface of a magnet or of a capacitor. This is due to abrupt changes of material properties on very small scales at the boundary of most technically relevant bodies. Here, it cannot be assumed *a priori* that $\boldsymbol{f}^{(\mathrm{EM})}$ is the correct force distribution as the total force in such a case is given by $\boldsymbol{F} = \int_\Omega \boldsymbol{f}^{(\mathrm{EM})}\,\mathrm{d}V + \int_{\partial\Omega} \boldsymbol{f}_I^{(\mathrm{EM})}\,\mathrm{d}A$. Solely the value of $\boldsymbol{F}$ can be compared to experiments. Here, the localization theorem cannot be applied as the integral types do not agree.

4 Electromagnetic force models

Over the years many force models have been introduced in the literature. The discussion began with the models presented in the papers of EINSTEIN and LAUB [9], MINKOWSKI [24], and ABRAHAM [1]. Another famous model was presented later by CHU et al. [6]. Other models are outlined in [15,26,39], *e.g.*, a generalized LORENTZ force model. In [16] modeling of the electromagnetic force is detailed by many examples, based on thermodynamical principals.

There is one specific case where everybody agrees upon the force: If magnetization and polarization vanish, the force density is given by the LORENTZ law in the form w.r.t. free charges and currents. This was well discussed in the work of TRUESDELL and TOUPIN [39, Sect. 284]. There is no consensus in academia which model is "correct" if magnetization and polarization are present; see the discussions in [3,5,12,21–23,28,33,40], among others. Often, this discussion is referred to as "ABRAHAM–MINKOWSKI controversy." However, this discussion may be misleading as it is by no means certain that any of these two models gives a correct prediction in an arbitrary situation.

Due to the vast number of models introduced in the literature, we only consider a selection of few. Most force models are based upon an initial postulate of the linear electromagnetic momentum density, $\boldsymbol{g}^{(\mathrm{EM})}$. Then, identities of vector calculus and MAXWELL's equations are used to find an *identity* of the form shown in Eq. (3.1). However, any such identity is not a unique representation. It is possible to transfer parts of the flux into the force density and *vice versa*. This will be demonstrated in a few examples. This is important to note as different identities imply different volume and surface force densities. The impact which this can have was demonstrated with local deformations in the *gedankenexperiment* of Sect. 2.

4.1 Generalized LORENTZ force model

In the work of TRUESDELL and TOUPIN [39, Sect. 284], the density of linear electromagnetic momentum was set to be $\boldsymbol{g}^{(\mathrm{EM})} = \boldsymbol{D} \times \boldsymbol{B}$ in the absence of any magnetization and polarization, so that a symmetric stress measure is obtained. A generalized LORENTZ force model assumes that this density is also valid if magnetization and polarization are present. The physical motivation behind this extension is the concept that the forces due to free and bound charges as well as currents are indistinguishable. More precisely, one assumes that the LORENTZ force model of free charges and currents is generalized by setting

$$q^{\mathrm{f}}\boldsymbol{E} + \boldsymbol{J}^{\mathrm{f}} \times \boldsymbol{B} \quad \rightarrow \quad q\,\boldsymbol{E} + \boldsymbol{J} \times \boldsymbol{B}.$$

This concept is commonly used in the work of I. MÜLLER and followers; see, *e.g.*, [26, Sect. 9.5], [27], or [13].

Using MAXWELL's equations, the MAXWELL–LORENTZ æther relations, and identities of vector calculus, the following identity can be obtained in an inertial frame:

$$\begin{aligned} \frac{\partial}{\partial t}(\boldsymbol{g}^{\mathrm{L}}) - \boldsymbol{\sigma}^{\mathrm{L}} = -\boldsymbol{f}^{\mathrm{L}}, \quad \text{with} \quad \boldsymbol{g}^{\mathrm{L}} = \boldsymbol{D} \times \boldsymbol{B}, \quad \boldsymbol{f}^{\mathrm{L}} = q\boldsymbol{E} + \boldsymbol{J} \times \boldsymbol{B}, \\ \boldsymbol{\sigma}^{\mathrm{L}} = -\tfrac{1}{2}(\epsilon_0 \boldsymbol{E} \cdot \boldsymbol{E} + \tfrac{1}{\mu_0}\boldsymbol{B} \cdot \boldsymbol{B})\mathbf{1} + \epsilon_0 \boldsymbol{E} \otimes \boldsymbol{E} + \tfrac{1}{\mu_0}\boldsymbol{B} \otimes \boldsymbol{B}. \end{aligned} \tag{4.1a}$$

As discussed before, a postulate of the momentum density does not yield a unique representation. However, without magnetization and polarization, the force must be $q^{\mathrm{f}}\boldsymbol{E} + \boldsymbol{J}^{\mathrm{f}} \times \boldsymbol{B}$. One now demands that the form of

the force remains, *i.e.*, q^{f} is exchanged by q and $\boldsymbol{J}^{\mathrm{f}}$ by $\boldsymbol{J}$. The flux defined above satisfies this requirement and is generally used in this model. One can also note that the obtained flux is symmetric.

By using the singular forms of MAXWELL's equations in Table 2 and some vector identities, one can find by evaluating Eq. (3.2) that

$$\boldsymbol{f}_I^{\mathrm{L}} = q_I\langle \boldsymbol{E}\rangle + \boldsymbol{J}_I \times \langle \boldsymbol{B}\rangle. \tag{4.1b}$$

The computations needed to obtain these representations of the forces are simple yet tedious. For this force model, the procedure is shown in Appendix C. For the following models, the computations are similar and therefore omitted.

4.2 ABRAHAM momentum density

The momentum density postulated by ABRAHAM reads

$$\boldsymbol{g}^{\mathrm{A}} = \boldsymbol{D} \times \mu_0 \mathfrak{H}.$$

By using MAXWELL's equations, the following relation can be derived:

$$\boldsymbol{g}^{\mathrm{A}} = \boldsymbol{D} \times \mu_0 \mathfrak{H} = \boldsymbol{D} \times (\boldsymbol{B} - \mu_0 \boldsymbol{M}) = \boldsymbol{g}^{\mathrm{L}} - \mu_0 \boldsymbol{D} \times \boldsymbol{M}.$$

For the fixed density, we can find infinitely many identities of the form

$$\frac{\partial}{\partial t}\boldsymbol{g}^{\mathrm{A}} - \nabla \cdot \boldsymbol{\sigma}^{\mathrm{A}_i} = -\boldsymbol{f}^{\mathrm{A}_i}.$$

The index i was introduced to distinguish the different choices for the flux and force density. For each choice, the flux and the force must be compatible, but it is always possible to transform parts of the flux to the force and *vice versa*. Therefore, there is no unique representation. In the following, we investigate two possibilities with an arbitrary symmetric and non-symmetric flux.

1. The symmetric choice of the flux $\boldsymbol{\sigma}^{\mathrm{A}_1} = \boldsymbol{\sigma}^{\mathrm{L}}$ yields the fixed forces:

$$\begin{aligned}
\boldsymbol{f}^{\mathrm{A}_1} &= q\boldsymbol{E} + \boldsymbol{J} \times \mu_0 \mathfrak{H} + (\nabla \times \boldsymbol{B}) \times \boldsymbol{M} + \mu_0 \boldsymbol{D} \times \frac{\partial \boldsymbol{M}}{\partial t}, \\
\boldsymbol{f}_I^{\mathrm{A}_1} &= q_I\langle \boldsymbol{E}\rangle + \boldsymbol{J}_I \times \mu_0 \langle \mathfrak{H}\rangle - \mu_0 w_\perp \langle \boldsymbol{D}\rangle \times [\![\boldsymbol{M}]\!] + (\boldsymbol{n} \times [\![\boldsymbol{B}]\!]) \times \langle \boldsymbol{M}\rangle.
\end{aligned}$$

2. The second choice made is to set $\boldsymbol{\sigma}^{\mathrm{A}_2} = \boldsymbol{\sigma}^{\mathrm{L}} - \boldsymbol{M} \otimes \boldsymbol{B}$, and the result reads:

$$\begin{aligned}
\boldsymbol{f}^{\mathrm{A}_2} &= q\boldsymbol{E} + \boldsymbol{J} \times \mu_0 \mathfrak{H} - \nabla \cdot (\boldsymbol{M} \otimes \boldsymbol{B}) + \mu_0 \boldsymbol{D} \times \frac{\partial \boldsymbol{M}}{\partial t}, \\
\boldsymbol{f}_I^{\mathrm{A}_2} &= q_I\langle \boldsymbol{E}\rangle + \boldsymbol{J}_I \times \mu_0 \langle \mathfrak{H}\rangle - \mu_0 w_\perp \langle \boldsymbol{D}\rangle \times [\![\boldsymbol{M}]\!] + \\
&\quad + (\boldsymbol{n} \times [\![\boldsymbol{B}]\!]) \times \langle \boldsymbol{M}\rangle - \boldsymbol{n} \cdot [\langle \boldsymbol{M}\rangle \otimes [\![\boldsymbol{B}]\!] + [\![\boldsymbol{M}]\!] \otimes \langle \boldsymbol{B}\rangle].
\end{aligned}$$

4.3 MINKOWSKI momentum density

The density proposed by MINKOWSKI reads

$$\boldsymbol{g}^{\mathrm{M}} = \mathfrak{D} \times \boldsymbol{B} = \boldsymbol{g}^{\mathrm{L}} + \boldsymbol{P} \times \boldsymbol{B}.$$

Again, there are infinitely many identities of the form

$$\frac{\partial}{\partial t}\boldsymbol{g}^{\mathrm{M}} - \nabla \cdot \boldsymbol{\sigma}^{\mathrm{M}_i} = -\boldsymbol{f}^{\mathrm{M}_i}.$$

Analogously to the ABRAHAM density above, we investigate an arbitrary symmetric and non-symmetric flux.

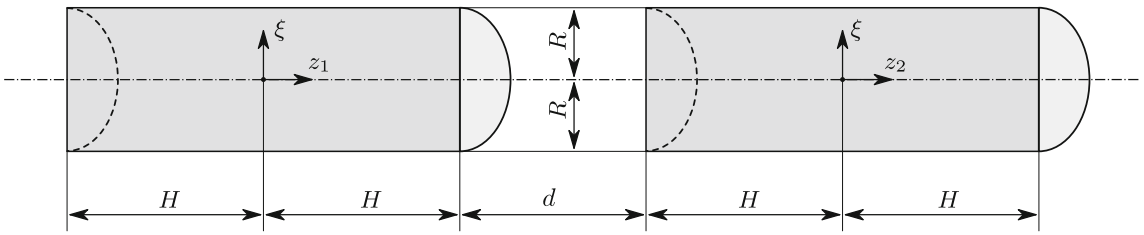

Fig. 3 Cross section and geometry of the analyzed cylindrical magnets

1. The symmetric choice of the flux: $\boldsymbol{\sigma}^{\mathrm{A}_1} = \boldsymbol{\sigma}^{\mathrm{L}}$ yields the fixed forces

$$\begin{aligned}\boldsymbol{f}^{\mathrm{M}_1} &= q\boldsymbol{E} + \boldsymbol{J}^{\mathrm{f}} \times \boldsymbol{B} + (\nabla \times \boldsymbol{M}) \times \boldsymbol{B} - (\nabla \times \boldsymbol{E}) \times \boldsymbol{P},\\ \boldsymbol{f}_I^{\mathrm{M}_1} &= q_I\langle \boldsymbol{E}\rangle + \boldsymbol{J}_I^{\mathrm{f}} \times \langle \boldsymbol{B}\rangle + \langle \boldsymbol{P}\rangle \times (\boldsymbol{n} \times [\![\boldsymbol{E}]\!]) + (\boldsymbol{n} \times [\![\boldsymbol{M}]\!]) \times \langle \boldsymbol{B}\rangle.\end{aligned}$$

2. The second choice made is to set $\boldsymbol{\sigma}^{\mathrm{M}_2} = \boldsymbol{\sigma}^{\mathrm{L}} + \boldsymbol{P} \otimes \boldsymbol{E} - \boldsymbol{B} \otimes \boldsymbol{M}$, and there results

$$\begin{aligned}\boldsymbol{f}^{\mathrm{M}_2} &= q^{\mathrm{f}}\boldsymbol{E} + \boldsymbol{J}^{\mathrm{f}} \times \boldsymbol{B} - (\nabla \otimes \boldsymbol{M}) \cdot \boldsymbol{B} + (\nabla \otimes \boldsymbol{E}) \cdot \boldsymbol{P},\\ \boldsymbol{f}_I^{\mathrm{M}_2} &= q_I^{\mathrm{f}}\langle \boldsymbol{E}\rangle + \boldsymbol{J}_I^{\mathrm{f}} \times \langle \boldsymbol{B}\rangle + \boldsymbol{n}(\langle \boldsymbol{P}\rangle \cdot [\![\boldsymbol{E}]\!] - \langle \boldsymbol{B}\rangle \cdot [\![\boldsymbol{M}]\!]).\end{aligned}$$

4.4 Einstein–Laub force model

The Einstein–Laub force model defines the momentum density, the flux, and the force by

$$\begin{aligned}\boldsymbol{g}^{\mathrm{EL}} &= \boldsymbol{D} \times \mu_0\mathfrak{H} = \boldsymbol{g}^{\mathrm{L}} - \boldsymbol{D} \times \mu_0\boldsymbol{M},\\ \boldsymbol{\sigma}^{\mathrm{EL}} &= -\tfrac{1}{2}(\epsilon_0\boldsymbol{E} \cdot \boldsymbol{E} + \mu_0\mathfrak{H} \cdot \mathfrak{H})\mathbf{1} + \mathfrak{D} \otimes \boldsymbol{E} + \boldsymbol{B} \otimes \mathfrak{H},\\ \boldsymbol{f}^{\mathrm{EL}} &= q^{\mathrm{f}}\boldsymbol{E} + \boldsymbol{J}^{\mathrm{f}} \times \mu_0\mathfrak{H} + \boldsymbol{P} \cdot (\nabla \otimes \boldsymbol{E}) + \frac{\partial \boldsymbol{P}}{\partial t} \times \mu_0\mathfrak{H} + \mu_0\boldsymbol{M} \cdot (\nabla \otimes \mathfrak{H}) - \mu_0\frac{\partial \boldsymbol{M}}{\partial t} \times \boldsymbol{D}.\end{aligned}$$

Due to Eq. (3.2), this also fixes the surface force. One finds that

$$\boldsymbol{f}_I^{\mathrm{EL}} = \boldsymbol{f}_I^{\mathrm{M}_2} + \boldsymbol{n}[\![\boldsymbol{B} \cdot \boldsymbol{M} - \tfrac{\mu_0}{2}\boldsymbol{M} \cdot \boldsymbol{M}]\!] - w_\perp[\![\mathfrak{D} \times \mu_0\boldsymbol{M} + \boldsymbol{P} \times \mu_0\mathfrak{H}]\!].$$

Note that this force model employs the same momentum density as the Abraham models.

5 An example of global effects: total force between two magnets

We consider two cylindrical ideal magnets possessing a constant homogeneous axial magnetization of strength M_0. Both cylinders have the same geometry and are coaxially aligned. We are interested in the total force acting between the two magnets as a function of the end-to-end distance d, *cf.* Fig. 3.

In this section, the force is computed employing each introduced force model above. The theoretical results are compared to each other and with conducted experimental data.

First, all force models are specialized for the magnetostatic case. At this stage, we are not interested in the deformation of the magnets and therefore ignore the self-field of a considered magnet. Such fields do not contribute to the total force, *i.e.*, a *perpetuum mobile* is not possible. It can be shown that their contributions vanish.

The magnetic fields of hollow cylinders, which are axially magnetized, are computed in [31]. The result can be specialized to a solid cylinder. For the magnetization direction, a factor β is introduced

$$\beta = \begin{cases} +1, & \boldsymbol{M} \cdot \boldsymbol{e}_z = +M_0,\\ -1, & \boldsymbol{M} \cdot \boldsymbol{e}_z = -M_0.\end{cases}$$

The magnetic field of one cylinder reads

$$\boldsymbol{B}(\tilde{\boldsymbol{x}}) = \mu_0 M_0 \beta \frac{1}{\pi} \sum_{\gamma=0}^{1} (-1)^\gamma \frac{1}{\sqrt{\mathcal{H}_\gamma^2}} \left[\frac{1}{k_\gamma^2} \left\{ (k_\gamma^2 - 2)\mathrm{K}(k_\gamma^2) + 2\mathrm{E}(k_\gamma^2) \right\} \boldsymbol{e}_\xi + \frac{\mathcal{Z}_\gamma}{2} \left\{ \frac{1-\tilde{\xi}}{1+\tilde{\xi}} \Pi(m^2, k_\gamma^2) + \mathrm{K}(k_\gamma^2) \right\} \boldsymbol{e}_z \right],$$

with

$$\mathcal{Z}_\gamma(\tilde{z}) = \tilde{z} + (-1)^\gamma \tilde{H}, \quad \mathcal{H}_\gamma^2(\tilde{\xi}, \tilde{z}) = 1 + 2\tilde{\xi} + \tilde{\xi}^2 + \mathcal{Z}_\gamma^2, \quad k_\gamma^2(\tilde{\xi}, \tilde{z}) = \frac{4\tilde{\xi}}{\mathcal{H}_\gamma^2}, \quad m^2(\tilde{\xi}) = \frac{4\tilde{\xi}}{(1+\tilde{\xi})^2}.$$

All quantities herein marked with tildes are normalized by R, *e.g.*, $\tilde{\xi} = \xi/R$, where ξ is the cylindrical radial coordinate. The occurring complete elliptic integrals are defined by

$$\mathrm{K}(k) = \int_{\varphi=0}^{\frac{\pi}{2}} \frac{1}{\sqrt{1 - k^2 \sin^2 \varphi}} \, \mathrm{d}\varphi, \quad \mathrm{E}(k) = \int_{\varphi=0}^{\frac{\pi}{2}} \sqrt{1 - k^2 \sin^2 \varphi} \, \mathrm{d}\varphi,$$

$$\Pi(m, k) = \int_{\varphi=0}^{\frac{\pi}{2}} \frac{1}{(1 - m \sin^2 \varphi)\sqrt{1 - k^2 \sin^2 \varphi}} \, \mathrm{d}\varphi.$$

Subsequently, we are interested in the magnetic field of the second magnet observed in the system of the first. Therefore, a coordinate transformation w.r.t. the axial direction is performed: $z_2 = z_1 - (2H + d)$. Defining $\kappa = d/R$, the magnetic field of the second magnet w.r.t. the coordinate system of the first reads

$$\boldsymbol{B}^{(2)}(\tilde{\xi}, \tilde{z}_1) = \boldsymbol{B}(\tilde{\xi}, \tilde{z}_1 - 2\tilde{H} - \kappa).$$

Note that $\tilde{\xi}$ is equal in both coordinate systems as the cylinders are coaxial.

5.1 Magnetostatic force specialization

In this situation, all time derivatives vanish. Furthermore, there are no polarization, no free charges, and no free currents. Because the magnetization is homogeneous corresponding spatial derivatives vanish. Also, the polarization charge $q^\mathrm{r} = -\nabla \cdot \boldsymbol{P}$, the polarization current $\partial \boldsymbol{P}/\partial t$, and the magnetization current $\nabla \times \boldsymbol{M}$ vanish. Therefore, $q = 0$ and $\boldsymbol{J} = \boldsymbol{0}$ in the magnets.

Since there is no polarizable medium outside the magnets, $q_l^\mathrm{r} = 0$. Since the magnets do not move, the surface polarization current $-[\![\boldsymbol{P}]\!] w_\perp$ vanishes also. However, there is a surface current due to magnetization, *i.e.*, $\boldsymbol{n} \times [\![\boldsymbol{M}]\!]$. Note that there are no electric charges in any region, and therefore, $\boldsymbol{E} \equiv \boldsymbol{0}$ everywhere.

Since MAXWELL's equations in a body at rest are linear, the total magnetic field can be decomposed w.r.t. the individual fields of the two cylinders. The superimposed field at any point in space reads $\boldsymbol{B}^{(12)} = \boldsymbol{B}^{(1)} + \boldsymbol{B}^{(2)}$. Since we are only interested in the total force acting on the first cylinder and not in the deformation of that cylinder, only the field $\boldsymbol{B}^{(2)}$ is of interested. This simplifies the analysis, and on the surface of the first cylinder, we have

$$[\![\boldsymbol{B}^{(2)}]\!] = \boldsymbol{0}, \quad \text{and} \quad \langle \boldsymbol{B}^{(2)} \rangle = \boldsymbol{B}^{(2)}, \quad \forall \boldsymbol{x} \in \partial\Omega_1.$$

Also, in Ω_1, $\boldsymbol{B}^{(2)} = \mu_0 \boldsymbol{H}^{(2)}$. Therefore, $\nabla \times \boldsymbol{B}^{(2)} = \boldsymbol{0}$ in this region. In what follows, we use a normalization $\boldsymbol{B}^{(2)} = \mu_0 M_0 \tilde{\boldsymbol{B}}^{(2)}$. Furthermore, the jump of the magnetization on the surface of the first cylinder $\partial\Omega_1$ is *a priori* known as $[\![\boldsymbol{M}]\!] = -M_0 \boldsymbol{e}_z$, where the magnetization of the first cylinder is always set in the positive z-direction.

The above stated force relations reduce to

$$
\begin{aligned}
\boldsymbol{f}^{\mathrm{L}} &= \boldsymbol{0},\\
\boldsymbol{f}_I^{\mathrm{L}} &= (\boldsymbol{n}\times[\![\boldsymbol{M}]\!])\times\langle\boldsymbol{B}\rangle = \mu_0 M_0^2(\boldsymbol{e}_z\times\boldsymbol{n})\times\tilde{\boldsymbol{B}}^{(2)},\\
\boldsymbol{f}^{\mathrm{A}_1} &= \boldsymbol{0},\\
\boldsymbol{f}_I^{\mathrm{A}_1} &= (\boldsymbol{n}\times[\![\boldsymbol{M}]\!])\times\langle\boldsymbol{B}-\mu_0\boldsymbol{M}\rangle + (\boldsymbol{n}\times[\![\boldsymbol{B}]\!])\times\langle\boldsymbol{M}\rangle\\
&= \mu_0 M_0^2(\boldsymbol{e}_z\times\boldsymbol{n})\times(\tilde{\boldsymbol{B}}^{(2)}-\tfrac{1}{2}\boldsymbol{e}_z),\\
\boldsymbol{f}^{\mathrm{A}_2} &= -\nabla\cdot(\boldsymbol{M}\otimes\boldsymbol{B}) = -\mu_0 M_0^2\nabla\cdot(\boldsymbol{e}_z\otimes\tilde{\boldsymbol{B}}^{(2)}),\\
\boldsymbol{f}_I^{\mathrm{A}_2} &= (\boldsymbol{n}\times[\![\boldsymbol{M}]\!])\times\langle\boldsymbol{B}-\mu_0\boldsymbol{M}\rangle + (\boldsymbol{n}\times[\![\boldsymbol{B}]\!])\times\langle\boldsymbol{M}\rangle - \boldsymbol{n}\cdot([\![\boldsymbol{M}]\!]\otimes\langle\boldsymbol{B}\rangle + \langle\boldsymbol{M}\rangle\otimes[\![\boldsymbol{B}]\!])\\
&= \mu_0 M_0^2[(\boldsymbol{e}_z\times\boldsymbol{n})\times(\tilde{\boldsymbol{B}}^{(2)}-\tfrac{1}{2}\boldsymbol{e}_z) + (\boldsymbol{n}\cdot\boldsymbol{e}_z)\tilde{\boldsymbol{B}}^{(2)}],\\
\boldsymbol{f}^{\mathrm{M}_1} &= \boldsymbol{0},\\
\boldsymbol{f}_I^{\mathrm{M}_1} &= (\boldsymbol{n}\times[\![\boldsymbol{M}]\!])\times\langle\boldsymbol{B}\rangle = \mu_0 M_0^2(\boldsymbol{e}_z\times\boldsymbol{n})\times\tilde{\boldsymbol{B}}^{(2)},\\
\boldsymbol{f}^{\mathrm{M}_2} &= \boldsymbol{0},\\
\boldsymbol{f}_I^{\mathrm{M}_2} &= -(\langle\boldsymbol{B}\rangle\cdot[\![\boldsymbol{M}]\!])\boldsymbol{n} = \mu_0 M_0^2\tilde{B}_z^{(2)}\boldsymbol{n},\\
\boldsymbol{f}^{\mathrm{EL}} &= \boldsymbol{M}\cdot(\nabla\otimes\mu_0\mathfrak{H}) = \nabla\cdot(\boldsymbol{M}\otimes\mu_0\mathfrak{H}) = \nabla\cdot(\boldsymbol{M}\otimes\boldsymbol{B})\\
&= \mu_0 M_0^2\nabla\cdot(\boldsymbol{e}_z\otimes\tilde{\boldsymbol{B}}^{(2)}),\\
\boldsymbol{f}_I^{\mathrm{EL}} &= \boldsymbol{f}_I^{\mathrm{M}_2} + \boldsymbol{n}[\![\boldsymbol{B}\cdot\boldsymbol{M} - \tfrac{\mu_0}{2}\boldsymbol{M}\cdot\boldsymbol{M}]\!] = -(\langle\boldsymbol{B}\rangle\cdot[\![\boldsymbol{M}]\!])\boldsymbol{n} + (\langle\boldsymbol{B}\rangle\cdot[\![\boldsymbol{M}]\!])\boldsymbol{n} - \boldsymbol{n}\tfrac{\mu_0}{2}[\![\boldsymbol{M}\cdot\boldsymbol{M}]\!]\\
&= \mu_0 M_0^2\tfrac{1}{2}\boldsymbol{n}.
\end{aligned}
$$

5.2 Theoretical axial force predictions

Now we proceed to compute the axial force for the individual models.

Generalized LORENTZ: The volume force density vanishes, and the surface density is only different from zero at the lateral surface. Therefore, we obtain

$$
\boldsymbol{F}^{\mathrm{L}} = \mu_0 M_0^2 R^2 \int_{\varphi=0}^{2\pi}\int_{\tilde{z}_1=-\tilde{H}}^{\tilde{H}} \boldsymbol{e}_\varphi\times\tilde{\boldsymbol{B}}^{(2)}\,\mathrm{d}\varphi\,\mathrm{d}\tilde{z}_1 = -\mu_0 M_0^2 R^2 2\pi\boldsymbol{e}_z\int_{\tilde{z}_1=-\tilde{H}}^{\tilde{H}}\tilde{B}_\xi^{(2)}(\tilde{\xi}=1,\tilde{z}_1)\,\mathrm{d}\tilde{z}_1,
$$

where any forces in the lateral directions were ignored because they cancel out due to azimuthal symmetry. In the following, we employ normalized forces, *i.e.*, $\boldsymbol{F} = \mu_0 M_0^2 R^2\tilde{\boldsymbol{F}}$. Therefore, we have a normalized axial force

$$
\tilde{F}_z^{\mathrm{L}} = -2\pi\int_{\tilde{z}_1=-\tilde{H}}^{\tilde{H}}\tilde{B}_\xi^{(2)}(\tilde{\xi}=1,\tilde{z}_1)\,\mathrm{d}\tilde{z}_1.
$$

This integral will be computed later.

Symmetric MINKOWSKI: For this special case, we immediately obtain

$$
\tilde{F}_z^{\mathrm{M}_1} = \tilde{F}_z^{\mathrm{L}},
$$

since the force densities in both models are equal.

Asymmetric MINKOWSKI: We find that only the surface density at the base areas do not vanish

$$\tilde{F}_z^{\mathrm{M}_2} = 2\pi \sum_{\gamma=0}^{1} (-1)^\gamma \int_{\tilde{\xi}=0}^{1} \tilde{B}_z^{(2)}(\tilde{\xi}, \tilde{z}_1 = (-1)^\gamma \tilde{H}) \tilde{\xi} \, \mathrm{d}\tilde{\xi}.$$

However, this integral can be rewritten using GAUSS' law and noting that

$$\begin{aligned} 0 &= \int_{\Omega_1} \nabla \cdot \tilde{\boldsymbol{B}}^{(2)} \, \mathrm{d}V = \oint_{\partial\Omega_1} \boldsymbol{n} \cdot \tilde{\boldsymbol{B}}^{(2)} \, \mathrm{d}A \\ &= 2\pi R^2 \int_{\tilde{z}_1=-\tilde{H}}^{\tilde{H}} \tilde{B}_{\tilde{\xi}}^{(2)}(\tilde{\xi}=1, \tilde{z}_1) \, \mathrm{d}\tilde{z}_1 + 2\pi R^2 \sum_{\gamma=0}^{1} (-1)^\gamma \int_{\tilde{\xi}=0}^{1} \tilde{B}_z^{(2)}(\tilde{\xi}, \tilde{z}_1 = (-1)^\gamma \tilde{H}) \tilde{\xi} \, \mathrm{d}\tilde{\xi}. \end{aligned} \tag{5.1}$$

Therefore, we obtain again the same result,

$$\tilde{F}_z^{\mathrm{M}_2} = \tilde{F}_z^{\mathrm{L}}.$$

Symmetric ABRAHAM: In this problem, only a force density on the lateral surface exists. Ignoring force components in the lateral directions as they cancel out by integration, we obtain

$$\tilde{F}_z^{\mathrm{A}_1} = \tilde{F}_z^{\mathrm{L}}.$$

Asymmetric ABRAHAM: First, we investigate the volume force

$$\begin{aligned} \int_{\Omega_1} \boldsymbol{f}^{\mathrm{A}_2} \, \mathrm{d}V &= -\mu_0 M_0^2 \int_{\Omega_1} \nabla \cdot (\boldsymbol{e}_z \otimes \tilde{\boldsymbol{B}}^{(2)}) \, \mathrm{d}V = -\mu_0 M_0^2 \oint_{\partial\Omega_1} \boldsymbol{n} \cdot (\boldsymbol{e}_z \otimes \tilde{\boldsymbol{B}}^{(2)}) \, \mathrm{d}A \\ &= -\mu_0 M_0^2 R^2 2\pi \boldsymbol{e}_z \sum_{\gamma=0}^{1} (-1)^\gamma \int_{\tilde{\xi}=0}^{1} \tilde{B}_z^{(2)}(\tilde{\xi}, \tilde{z}_1 = (-1)^\gamma \tilde{H}) \tilde{\xi} \, \mathrm{d}\tilde{\xi} = -\mu_0 M_0^2 R^2 \tilde{F}_z^{\mathrm{L}} \boldsymbol{e}_z, \end{aligned}$$

in which lateral components are neglected. The analysis of the surface force yields

$$\begin{aligned} \oint_{\partial\Omega_1} \boldsymbol{f}_I^{\mathrm{A}_2} \, \mathrm{d}A &= -\mu_0 M_0^2 2\pi R^2 \boldsymbol{e}_z \int_{\tilde{z}_1=-\tilde{H}}^{\tilde{H}} \tilde{B}_{\tilde{\xi}}^{(2)}(\tilde{\xi}=1, \tilde{z}_1) \, \mathrm{d}\tilde{z}_1 \\ &\quad + \mu_0 M_0^2 2\pi R^2 \sum_{\gamma=0}^{1} (-1)^\gamma \int_{\tilde{\xi}=0}^{1} \tilde{B}_z^{(2)}(\tilde{\xi}, \tilde{z}_1 = (-1)^\gamma \tilde{H}) \tilde{\xi} \, \mathrm{d}\tilde{\xi} = 2\mu_0 M_0^2 R^2 \tilde{F}_z^{\mathrm{L}} \boldsymbol{e}_z, \end{aligned}$$

owing to Eq. (5.1). Hence,

$$\tilde{F}_z^{\mathrm{A}_2} = \tilde{F}_z^{\mathrm{L}}.$$

EINSTEIN–LAUB: By comparing the volume force densities of this model with the corresponding expression of the asymmetric ABRAHAM case studied above, we immediately have

$$\int_{\Omega_1} \boldsymbol{f}^{\mathrm{EL}} \, \mathrm{d}V = \mu_0 M_0^2 R^2 \tilde{F}_z^{\mathrm{L}} \boldsymbol{e}_z.$$

On the surface, the integrated force vanishes. Hence,

$$\tilde{F}_z^{\mathrm{EL}} = \tilde{F}_z^{\mathrm{L}}.$$

5.3 Analytical solution

Remarkably, all force models yield the same total force acting on the considered magnet. That the total electromagnetic force that acts on a body is the same for many electromagnetic force models in many situations has been noted in the literature before, *cf.* [29] and [16, Chap. 3]. Here, the analytical solution of all models reduces to computing the integral

$$\tilde{F}_z = -2\pi \int_{\tilde{z}_1=-\tilde{H}}^{\tilde{H}} \tilde{B}_\xi^{(2)}(\tilde{\xi}=1,\tilde{z}_1)\,\mathrm{d}\tilde{z}_1, \quad \text{or:} \quad \tilde{F}_z = 2\pi \sum_{\gamma=0}^{1}(-1)^\gamma \int_{\tilde{\xi}=0}^{1} \tilde{B}_z^{(2)}(\tilde{\xi},\tilde{z}_1=(-1)^\gamma\tilde{H})\tilde{\xi}\,\mathrm{d}\tilde{\xi}.$$

In the following, the former integral is considered. The normalized radial field component of the second magnet is given by

$$\tilde{B}_\xi^{(2)}(\tilde{\xi},\tilde{z}_1) = \tilde{B}_\xi(\tilde{\xi},\tilde{z}_1-2\tilde{H}-\kappa), \quad \tilde{B}_\xi(\tilde{\xi},\tilde{z}) = \beta\frac{1}{\pi}\sum_{\gamma=0}^{1}(-1)^\gamma \frac{1}{\sqrt{\mathcal{H}_\gamma^2}}\frac{1}{k_\gamma^2}\Big\{(k_\gamma^2-2)\mathrm{K}(k_\gamma^2)+2\mathrm{E}(k_\gamma^2)\Big\}.$$

On the lateral surface, we have $\tilde{\xi}=1$, and find

$$\mathcal{Z}_\gamma(\tilde{z}) = \tilde{z}+(-1)^\gamma\tilde{H}, \quad k_\gamma^2(1,\tilde{z}) = \tfrac{4}{\mathcal{H}_\gamma^2}, \quad \mathcal{H}_\gamma^2(1,\tilde{z}) = 4+\mathcal{Z}_\gamma^2 = \frac{4}{k_\gamma^2},$$

so that

$$\sqrt{\mathcal{H}_\gamma^2(1,\tilde{z})}k_\gamma^2(1,\tilde{z}) = 2\sqrt{k_\gamma^2(1,\tilde{z})}.$$

In this special case, the modulus k_γ^2 is only a function of $\tilde{z}$, so we can set $h_\gamma(\tilde{z}) := k_\gamma^2(1,\tilde{z})$. With this, the integral reads

$$\tilde{F}_z = -\beta\sum_{\gamma=0}^{1}(-1)^\gamma \int_{\tilde{z}_1=-\tilde{H}}^{\tilde{H}} \frac{1}{\sqrt{h_\gamma(\tilde{z}_2)}}\Big\{(h_\gamma(\tilde{z}_2)-2)\mathrm{K}(h_\gamma(\tilde{z}_2))+2\mathrm{E}(h_\gamma(\tilde{z}_2))\Big\}\,\mathrm{d}\tilde{z}_1, \quad \text{where} \quad \tilde{z}_2 = \tilde{z}_1-2\tilde{H}-\kappa.$$

This integral $\tilde{F}_z$ can be transformed by using

$$\mathrm{d}h_\gamma = \frac{\partial h_\gamma}{\partial\mathcal{Z}_\gamma}\frac{\partial\mathcal{Z}_\gamma}{\partial\tilde{z}_2}\frac{\partial\tilde{z}_2}{\partial\tilde{z}_1}\mathrm{d}\tilde{z}_1 = \sqrt{h_\gamma^3-h_\gamma^4}\,\mathrm{d}\tilde{z}_1 \quad\Leftrightarrow\quad \mathrm{d}\tilde{z}_1 = \frac{1}{\sqrt{h_\gamma^3-h_\gamma^4}}\mathrm{d}h_\gamma,$$

where the proper sign has been determined by noting that $\mathcal{Z}_\gamma(\tilde{z}_2(\tilde{z}_1)) < 0$ for $\tilde{z}_1 \in [-\tilde{H},\tilde{H}]$. Therefore,

$$\tilde{F}_z = -\beta\sum_{\gamma=0}^{1}(-1)^\gamma \int_{h_\gamma=\Psi_{\gamma 0}}^{\Psi_{\gamma 1}} \Big\{(h_\gamma-2)\mathrm{K}(h_\gamma)+2\mathrm{E}(h_\gamma)\Big\}\frac{1}{h_\gamma^2\sqrt{1-h_\gamma}}\mathrm{d}h_\gamma, \tag{5.2}$$

where

$$\Psi_{\gamma\delta} = \frac{4}{4+(-(-1)^\delta\tilde{H}-2\tilde{H}-\kappa+(-1)^\gamma\tilde{H})^2} = \frac{4}{4+([(-1)^\delta-(-1)^\gamma+2]\tilde{H}+\kappa)^2}.$$

The integral can be solved by using the series representations of the elliptic integrals, *i.e.*,

$$\mathrm{K}(h) = \frac{\pi}{2}\sum_{n=0}^{\infty}P_{2n}^2(0)h^n, \quad \mathrm{E}(h) = \frac{\pi}{2}\sum_{n=0}^{\infty}\frac{P_{2n}^2(0)}{1-2n}h^n,$$

where P_n denotes the nth LEGENDRE polynomial; see [11]. By acknowledging the series representation, the integral reads

$$\tilde{F}_z = -\beta\frac{\pi}{2}\sum_{n=0}^{\infty} P_{2n}^2(0)\sum_{\gamma=0}^{1}(-1)^{\gamma}\int_{h_\gamma=\Psi_{\gamma 0}}^{\Psi_{\gamma 1}}\left\{h_\gamma+\frac{4n}{1-2n}\right\}\frac{h_\gamma^{n-2}}{\sqrt{1-h_\gamma}}\mathrm{d}h_\gamma.$$

Noting that

$$\operatorname{artanh}(x) = \tfrac{1}{2}[\ln(1+x)-\ln(1-x)],$$

the arising integrals can be solved by analyzing the cases $n=0$ and $n=1$ first,

$$\begin{aligned}(n=0):\quad \int_{h_\gamma=\Psi_{\gamma 0}}^{\Psi_{\gamma 1}}\frac{h_\gamma^{-1}}{\sqrt{1-h_\gamma}}\mathrm{d}h_\gamma &= -\sum_{\delta=0}^{1}(-1)^{\delta}[\ln(1-\sqrt{1-\Psi_{\gamma\delta}})-\ln(1+\sqrt{1-\Psi_{\gamma\delta}})]\\ &= 2\sum_{\delta=0}^{1}(-1)^{\delta}\operatorname{artanh}(\sqrt{1-\Psi_{\gamma\delta}}),\\ (n=1):\quad \int_{h_\gamma=\Psi_{\gamma 0}}^{\Psi_{\gamma 1}}\{h_\gamma-4\}\frac{h_\gamma^{-1}}{\sqrt{1-h_\gamma}}\mathrm{d}h_\gamma &= 2\sum_{\delta=0}^{1}(-1)^{\delta}[\sqrt{1-\Psi_{\gamma\delta}}-4\operatorname{artanh}(\sqrt{1-\Psi_{\gamma\delta}})].\end{aligned}$$

For $n>1$, we employ a coordinate transformation $g_\gamma = 1-h_\gamma$, so that

$$\begin{aligned}(n>1):\quad \int_{h_\gamma=\Psi_{\gamma 0}}^{\Psi_{\gamma 1}}\left\{h_\gamma+\frac{4n}{1-2n}\right\}\frac{h_\gamma^{n-2}}{\sqrt{1-h_\gamma}}\mathrm{d}h_\gamma &= -\int_{g_\gamma=1-\Psi_{\gamma 0}}^{1-\Psi_{\gamma 1}}\left\{1-g_\gamma+\frac{4n}{1-2n}\right\}\frac{(1-g_\gamma)^{n-2}}{\sqrt{g_\gamma}}\mathrm{d}g_\gamma\\ &= \sum_{\delta=0}^{1}(-1)^{\delta}\int_{g_\gamma=0}^{1-\Psi_{\gamma\delta}}\left\{1-g_\gamma+\frac{4n}{1-2n}\right\}\frac{(1-g_\gamma)^{n-2}}{\sqrt{g_\gamma}}\mathrm{d}g_\gamma.\end{aligned}$$

The integral in the so-obtained form can be solved in terms of incomplete beta functions, defined by

$$\mathrm{B}(x;a,b) := \int_{u=0}^{x} u^{a-1}(1-u)^{b-1}\,\mathrm{d}u,\quad x\le 1\wedge a>0.$$

By using this function, we find that for any $n>1$

$$\begin{aligned}&\sum_{\delta=0}^{1}(-1)^{\delta}\int_{g_\gamma=0}^{1-\Psi_{\gamma\delta}}\left\{1-g_\gamma+\frac{4n}{1-2n}\right\}\frac{(1-g_\gamma)^{n-2}}{\sqrt{g_\gamma}}\mathrm{d}g_\gamma\\ &\quad=\sum_{\delta=0}^{1}(-1)^{\delta}[\mathrm{B}(1-\Psi_{\gamma\delta};\tfrac{1}{2},n)+\tfrac{4n}{1-2n}\mathrm{B}(1-\Psi_{\gamma\delta};\tfrac{1}{2},n-1)].\end{aligned}$$

Hence, the problem is solved. However, for a more convenient representation, it is advantageous to introduce the hypergeometric function ${}_2\mathrm{F}_1$ by

$${}_2\mathrm{F}_1(a,b;c;z) := \sum_{n=0}^{\infty}\frac{(a)_n(b)_n}{(c)_n}\frac{z^n}{n!},$$

where $(\cdot)_n$ denote POCHHAMMER symbols; see [2, p. 256]. The incomplete beta functions are related to this function by

$$\mathrm{B}(x;a,b) = \frac{x^a}{a}\,{}_2\mathrm{F}_1(a,1-b;a+1;x), \quad \text{so that}$$
$$\frac{\mathrm{B}(1-\Psi_{\gamma\delta};\frac{1}{2},n)}{2\sqrt{1-\Psi_{\gamma\delta}}} = {}_2\mathrm{F}_1(\tfrac{1}{2},1-n;\tfrac{3}{2};1-\Psi_{\gamma\delta}),$$
$$\frac{\mathrm{B}(1-\Psi_{\gamma\delta};\frac{1}{2},n-1)}{2\sqrt{1-\Psi_{\gamma\delta}}} = {}_2\mathrm{F}_1(\tfrac{1}{2},2-n;\tfrac{3}{2};1-\Psi_{\gamma\delta}).$$

Also, we can note that

$${}_2\mathrm{F}_1(\tfrac{1}{2},0;\tfrac{3}{2};x) = 1, \qquad \sqrt{x}\,{}_2\mathrm{F}_1(\tfrac{1}{2},1;\tfrac{3}{2};x) = \operatorname{artanh}(\sqrt{x}).$$

Therefore, we obtain the scaled force function as

$$\tilde{F}_z(\kappa) = -\beta\pi \sum_{n=0}^{\infty}\sum_{\gamma=0}^{1}\sum_{\delta=0}^{1}(-1)^{\gamma+\delta}P_{2n}^2(0)\sqrt{1-\Psi_{\gamma\delta}(\kappa)}\,\star$$
$$\star\Big[{}_2\mathrm{F}_1(\tfrac{1}{2},1-n;\tfrac{3}{2};1-\Psi_{\gamma\delta}(\kappa)) + \tfrac{4n}{1-2n}\,{}_2\mathrm{F}_1(\tfrac{1}{2},2-n;\tfrac{3}{2};1-\Psi_{\gamma\delta}(\kappa))\Big], \tag{5.3a}$$

where the geometry function is given by

$$\Psi_{\gamma\delta}(\kappa) = \frac{4}{4+([(-1)^\delta-(-1)^\gamma+2]\tilde{H}+\kappa)^2}. \tag{5.3b}$$

The symbol $\star$ in Eq. (5.3a) is typeset to indicate that a scalar multiplication of the two lines is performed. The factor β is $+1$ if the magnetizations of the two magnets show in the same direction, *i.e.*, attraction forces are considered. For repelling forces, set $\beta = -1$. In order to obtain the force in physical dimensions, multiply $\tilde{F}_z(\kappa)$ by the force amplitude $\mu_0 M_0^2 R^2$. To employ distances in physical dimensions, substitute $\kappa = {}^d/_R$ and $\tilde{H} = {}^H/_R$.

To analyze this series solution, we consider a numerical solution $\tilde{F}_z^{\mathrm{num}}$ obtained by means of numerical integration of Eq. (5.2) with Mathematica, *cf.* [41]. In practical computations with the series solution, the sum over n is cut off at some $n_{\max}$. In Fig. 4a, it can be seen that series solution converges fast to the numerically obtained solution in the far field. However, in order to obtain a good result for the contact force, a high number $n_{\max}$ must be chosen. In order to evaluate convergence in this region, the relative error

$$e_{\mathrm{rel}}(n_{\max}) = \left|\tilde{F}_z(\kappa=0,n_{\max}) - \tilde{F}_z^{\mathrm{num}}(\kappa=0)\right| \left|\tilde{F}_z^{\mathrm{num}}(\kappa=0)\right|^{-1}$$

is shown in a double-logarithmic plot in Fig. 4b. It can be seen that the order of convergence is approximately $1/2$ in this region.

5.4 Comparison to experiment

In order to verify formula (5.3), measurements with equal cylindrical neodymium magnets were conducted, *cf.* [20]. The cylinders are axially magnetized as used in the analytical scenario above. The relevant properties of the magnets are listed in Table 1.

The total force for varying distances between the magnets is to be measured. Here, a microtensile testing machine MTS Tytron$^{\mathrm{TM}}$ 250 is used, *cf.* [25]. In order to limit near-field magnetic disturbances, the magnets are fixed inside plastic holders with epoxy resin. The holders are connected to rigid aluminum distance rods that are connected to the testing machine. This way, the disturbances of the immediate neighborhood of the magnets are negligible. The experiment is shown in Fig. 5.

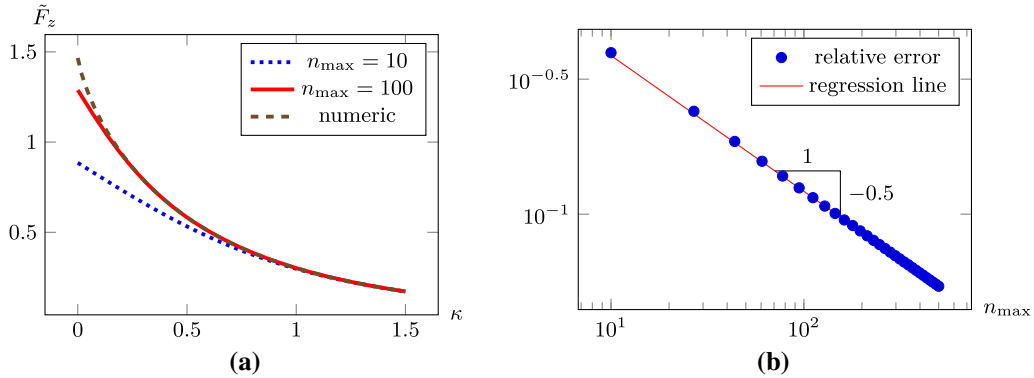

Fig. 4 Visualization of the analytical series solution and numerical integration solution of the axial force. They are plotted for varying κ in **a**. In **b**, the convergence of the contact force ($\kappa = 0$) is investigated. **a** Series solution of the axial force of Eq. (5.3) with different $n_{\max}$ and the result of the numerical integration of Eq. (5.2). **b** Relative error of the analytical contact force w.r.t. the numerical solution

Table 1 Selected properties of the magnets according to [20]

Property	Value
Total axial length $2H$	34.00 mm
Diameter $2R$	20.00 mm
Geometrical tolerance	±0.10 mm
Remanence $\mu_0 M_0$	(1.32–1.37) T

Fig. 5 Visualization of the axial force measurement. **a** A magnet in a plastic holder, connected to an aluminum distance rod. **b** Measurement of the forces with a microtensile testing machine

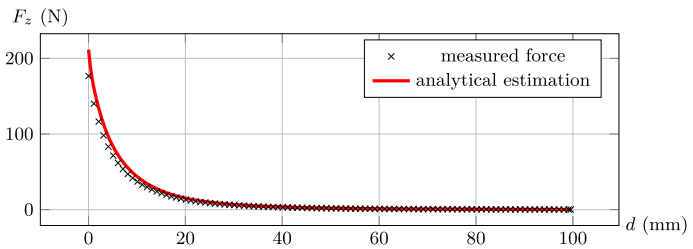

Fig. 6 Visualization of a reduced number of measurement points and the *a priori* estimation with the analytical solution

Both magnets are installed unidirectionally w.r.t. the magnetization in order to obtain (positive) traction forces, *i.e.*, $\beta = 1$ in Eq. (5.3). For a first test of the formula, a mean remanence of 1.35 T is used, and $R = 10$ mm. Hence, the force amplitude can be estimated to be ≈ 145 N. According to the table, $\tilde{H} = 1.7$. With this estimated force amplitude and geometry, the force between the magnets can be computed via Eq. (5.3). In Fig. 6, measured forces and the analytical estimations are plotted.

It can be seen that the estimation yields good results if the magnets are not too close to each other. In order to obtain better results for small gaps between the magnets and to see whether the form function of Eq. (5.3) describes the problem accurately, we assume that (a) the amplitude $\mu_0 M_0^2 R^2$ differs from the estimated value

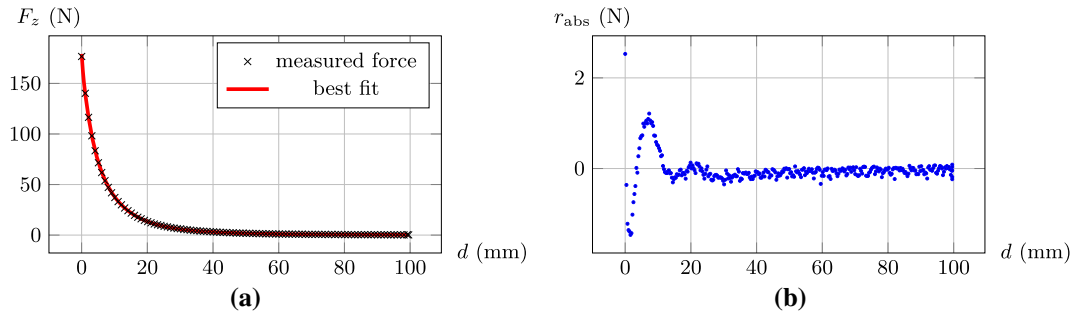

Fig. 7 Visualization of a reduced number of measurement points and the analytical solution with fitted parameters in (**a**). In **b**, the residuals of the measured data and the fitted solution are shown. In order not to clutter the plots, only a limited number of measurement points is shown. **a** Measured data and the best fit solution. **b** Residuals to measured data

and that (b) there may be a (small) axial position error. This error may be introduced in the measurement or can be caused by manufacturing tolerances, as given in Table 1. The assumption (b) is important as the form function is steep for small values of d. Therefore, we introduce the following function with two degrees of freedom:

$$F_z^{\text{fit}}(d, \mathcal{A}, \mathcal{X}) = \mathcal{A}\tilde{F}_z((d-\mathcal{X})/R),$$

where $\mathcal{A}$ is the (unknown) force amplitude and $\mathcal{X}$ is an (unknown) axial position error. We take $R = 10\,\text{mm}$ as given by Table 1. A nonlinear model fit is performed with Mathematica to obtain these parameters using the measured data. The best fit result yields $\mathcal{A} = 128.2\,\text{N}$ and $\mathcal{X} = -0.12\,\text{mm}$. The fitted force function is in good agreement with the measured data as can be seen in Fig. 7. In order to evaluate the quality of the result, an absolute residual $r_{\text{abs}} = F_z^{\text{fit}} - F_z^{\text{meas.}}$ is regarded also in the figure.

As can be seen in the figure, the form of the force function given in Eq. (5.3) describes the physical situation well. Even in the near-field, the residuals are small in comparison with the total force values. In this region, many errors may accumulate: angle and position errors in the measurement, the magnets may not be homogeneous as assumed, the magnetization of the material may possess a small field dependency, *etc*. However, if the forces are not of interest for small gaps between the magnets, the *a priori* estimation obtained via Table 1 and Eq. (5.3) yields good results, as can be seen Fig. 6.

5.5 Discussion of the axial force analysis

From the computations and measurements performed in this section, we conclude for the considered example of the magnets that

1. all considered models yield the same theoretical prediction, and
2. the prediction is in good agreement with the measurements.

The fact that in many situations various force models yield the same total force has been noticed in the literature before, *e.g.*, [4]. This gives rise to the question as to whether the *total* electromagnetic force is equal for all conceivable force models for every material and every (dynamical) situation. This question is not investigated any further here.

Since many force models lead to the same total force, the exact local force structure is often deemed unimportant. However, from the perspective of continuum mechanics, it is clear that, in general, different loading distributions for the same total force yield different deformations. Therefore, we shall analyze in the following sections the local effects of the force models.

6 An example of local effects: magnetostriction with selected force models

In order to analyze local effects of the previously introduced electromagnetic force models, we investigate another problem of magnetostatics. A permanent magnetic sphere of radius R with uniform magnetization, $\boldsymbol{M} = M_0\boldsymbol{e}_z$, is considered. Also, this magnet is isotropically linear-elastic, with LAMÉ parameters λ and μ. Depending on the considered force model, the magnetic field of the magnet gives rise to local forces acting

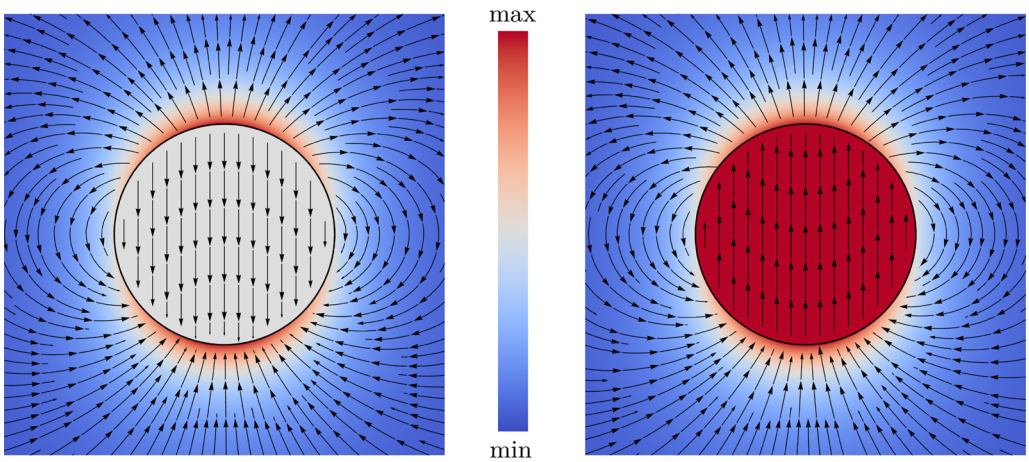

Fig. 8 Streamlines of the fields $\mathfrak{H}$ and $\boldsymbol{B}$ of a uniformly magnetized sphere. Colors indicate the norm of the corresponding field. The geometry of the sphere is outlined in black. **a** Free current potential $\mathfrak{H}$. **b** Magnetic flux density $\boldsymbol{B}$

in the volume and on the surface. Because the magnet cannot accelerate itself, the total force is zero for all models.

The solution of the magnetic field is well known,

$$\boldsymbol{B}^{\mathrm{I}} = \frac{2}{3}\mu_0 M_0 \left(P_1(x)\boldsymbol{e}_r + \frac{\mathrm{d}P_1(x)}{\mathrm{d}\vartheta}\boldsymbol{e}_\vartheta \right) = \frac{2}{3}\mu_0 M_0 (\cos\vartheta \boldsymbol{e}_r - \sin\vartheta \boldsymbol{e}_\vartheta), \tag{6.1a}$$

$$\boldsymbol{B}^{\mathrm{O}} = \frac{2}{3}\mu_0 M_0 \tilde{r}^{-3} \left(P_1(x)\boldsymbol{e}_r - \frac{1}{2}\frac{\mathrm{d}P_1(x)}{\mathrm{d}\vartheta}\boldsymbol{e}_\vartheta \right) = \frac{2}{3}\mu_0 M_0 \tilde{r}^{-3} (\cos\vartheta \boldsymbol{e}_r + \tfrac{1}{2}\sin\vartheta \boldsymbol{e}_\vartheta), \tag{6.1b}$$

where $\tilde{r} = r/R$ is the dimensionless radial spherical coordinate and $x = \cos\vartheta$. The index I denotes the interior of the magnet and O the exterior of the magnet. This solution is obtained in many textbooks on electromagnetism, *e.g.*, [10,17,37]. A visualization of the fields is given in Fig. 8.

6.1 Specialization of the local force densities

For the considered case of static magnetostriction, one can start by noting that the magnetic flux and free current potential are linear in the magnetization and therefore also homogeneous in the interior:

$$\boldsymbol{B}^{\mathrm{I}} = \tfrac{2}{3}\mu_0 \boldsymbol{M}, \qquad \mathfrak{H}^{\mathrm{I}} = -\tfrac{1}{3}\boldsymbol{M}\ ;$$

therefore, any derivative of these fields vanishes. We can also note that the charge and current densities reduce to

$$q = q^{\mathrm{f}} - \nabla\cdot\boldsymbol{P} = 0, \qquad q_I = q_I^{\mathrm{f}} - \boldsymbol{n}\cdot[\![\boldsymbol{P}]\!] = 0,$$
$$\boldsymbol{J} = \boldsymbol{J}^{\mathrm{f}} + \frac{\partial \boldsymbol{P}}{\partial t} + \nabla\times\boldsymbol{M} = \boldsymbol{0}, \qquad \boldsymbol{J}_I = \boldsymbol{J}_I^{\mathrm{f}} - [\![\boldsymbol{P}]\!]w_\perp + \boldsymbol{n}\times[\![\boldsymbol{M}]\!] = \boldsymbol{n}\times[\![\boldsymbol{M}]\!].$$

In the first step, the force densities of the models introduced in Sect. 4 are reduced by using the relations from above to read

$$\begin{aligned}
\boldsymbol{f}^{\mathrm{L}} &= \boldsymbol{0}, & \boldsymbol{f}_I^{\mathrm{L}} &= (\boldsymbol{n}\times[\![\boldsymbol{M}]\!])\times\langle\boldsymbol{B}\rangle,\\
\boldsymbol{f}^{\mathrm{A}_1} &= \boldsymbol{0}, & \boldsymbol{f}_I^{\mathrm{A}_1} &= (\boldsymbol{n}\times[\![\boldsymbol{M}]\!])\times\mu_0\langle\mathfrak{H}\rangle + (\boldsymbol{n}\times[\![\boldsymbol{B}]\!])\times\langle\boldsymbol{M}\rangle,\\
\boldsymbol{f}^{\mathrm{A}_2} &= \boldsymbol{0}, & \boldsymbol{f}_I^{\mathrm{A}_2} &= (\boldsymbol{n}\times[\![\boldsymbol{M}]\!])\times\mu_0\langle\mathfrak{H}\rangle + (\boldsymbol{n}\times[\![\boldsymbol{B}]\!])\times\langle\boldsymbol{M}\rangle - \boldsymbol{n}\cdot[\langle\boldsymbol{M}\rangle\otimes[\![\boldsymbol{B}]\!] + [\![\boldsymbol{M}]\!]\otimes\langle\boldsymbol{B}\rangle],\\
\boldsymbol{f}^{\mathrm{M}_1} &= \boldsymbol{0}, & \boldsymbol{f}_I^{\mathrm{M}_1} &= (\boldsymbol{n}\times[\![\boldsymbol{M}]\!])\times\langle\boldsymbol{B}\rangle,\\
\boldsymbol{f}^{\mathrm{M}_2} &= \boldsymbol{0}, & \boldsymbol{f}_I^{\mathrm{M}_2} &= -\boldsymbol{n}(\langle\boldsymbol{B}\rangle\cdot[\![\boldsymbol{M}]\!]),\\
\boldsymbol{f}^{\mathrm{EL}} &= \boldsymbol{0}, & \boldsymbol{f}_I^{\mathrm{EL}} &= -\boldsymbol{n}(\langle\boldsymbol{B}\rangle\cdot[\![\boldsymbol{M}]\!]) + \boldsymbol{n}[\![\boldsymbol{B}\cdot\boldsymbol{M} - \tfrac{\mu_0}{2}\boldsymbol{M}\cdot\boldsymbol{M}]\!].
\end{aligned}$$

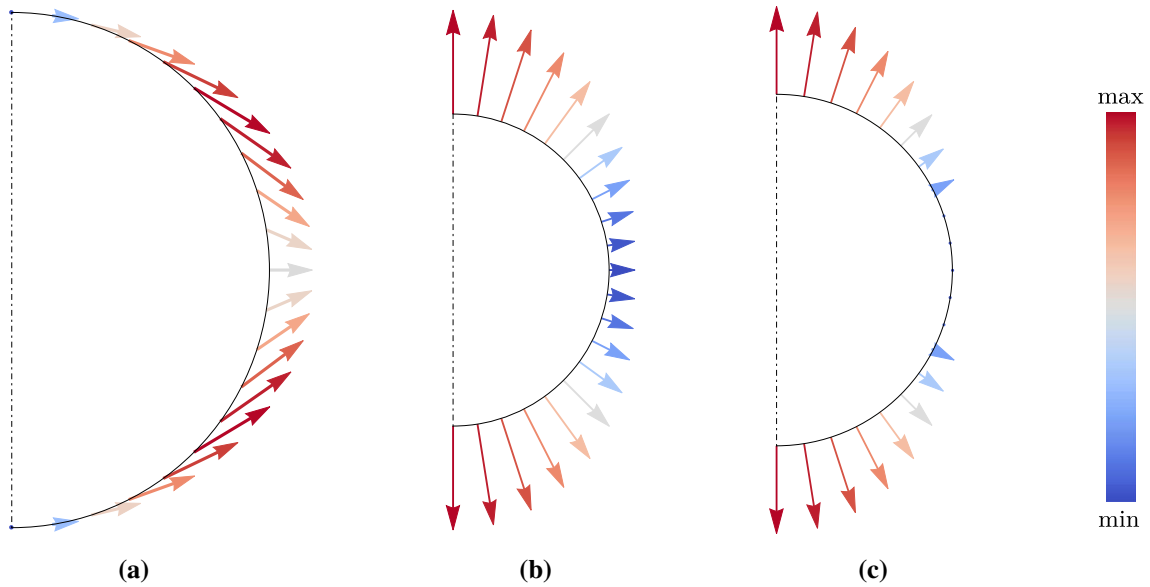

Fig. 9 Qualitative representations of the surface force densities. In **c**, arrows are suppressed for small force magnitudes

We note that all volumetric force densities vanish. However, the local force densities on the surface may differ. In the next step, the contained jump and mean value operators are specialized for the considered case and yield

$$\begin{aligned}
\langle \boldsymbol{B} \rangle &= \tfrac{1}{6}\mu_0 M_0 (4\cos\vartheta \boldsymbol{e}_r - \sin\vartheta \boldsymbol{e}_\vartheta), \quad [\![\boldsymbol{B}]\!] = \mu_0 M_0 \sin\vartheta \boldsymbol{e}_\vartheta, \\
\langle \mathfrak{H} \rangle &= \frac{M_0}{6}(\cos\vartheta \boldsymbol{e}_r + 2\sin\vartheta \boldsymbol{e}_\vartheta), \quad [\![\mathfrak{H}]\!] = M_0 \cos\vartheta \boldsymbol{e}_r, \\
\langle \boldsymbol{M} \rangle &= \tfrac{1}{2} M_0 \boldsymbol{e}_z, \quad [\![\boldsymbol{M}]\!] = -M_0 \boldsymbol{e}_z, \quad [\![\boldsymbol{B}\cdot\boldsymbol{M} - \tfrac{\mu_0}{2}\boldsymbol{M}\cdot\boldsymbol{M}]\!] = -\tfrac{1}{6}\mu_0 M_0^2.
\end{aligned}$$

By using these relations, the surface densities reduce and read with $\boldsymbol{n} = \boldsymbol{e}_r$, explicitly

$$\begin{aligned}
\boldsymbol{f}_I^{\mathrm{L}} &= \tfrac{1}{6}\mu_0 M_0^2 (\sin^2\vartheta \boldsymbol{e}_r + 4\sin\vartheta\cos\vartheta \boldsymbol{e}_\vartheta) = \boldsymbol{f}_I^{(1)}, \\
\boldsymbol{f}_I^{\mathrm{A}_1} &= \tfrac{1}{6}\mu_0 M_0^2 (\sin^2\vartheta \boldsymbol{e}_r + 4\sin\vartheta\cos\vartheta \boldsymbol{e}_\vartheta) = \boldsymbol{f}_I^{(1)}, \\
\boldsymbol{f}_I^{\mathrm{A}_2} &= \tfrac{1}{6}\mu_0 M_0^2 (1 + 3\cos^2\vartheta) \boldsymbol{e}_r = \boldsymbol{f}_I^{(2)}, \\
\boldsymbol{f}_I^{\mathrm{M}_1} &= \tfrac{1}{6}\mu_0 M_0^2 (\sin^2\vartheta \boldsymbol{e}_r + 4\sin\vartheta\cos\vartheta \boldsymbol{e}_\vartheta) = \boldsymbol{f}_I^{(1)}, \\
\boldsymbol{f}_I^{\mathrm{M}_2} &= \tfrac{1}{6}\mu_0 M_0^2 (1 + 3\cos^2\vartheta) \boldsymbol{e}_r = \boldsymbol{f}_I^{(2)}, \\
\boldsymbol{f}_I^{\mathrm{EL}} &= \tfrac{1}{2}\mu_0 M_0^2 \cos^2\vartheta \boldsymbol{e}_r = \boldsymbol{f}_I^{(3)}.
\end{aligned}$$

In this special case, all models with (the same) symmetric stress measure yield the same surface force density. Interestingly, the considered non-symmetric ABRAHAM and MINKOWSKI models also coincide for this magnetic problem. The EINSTEIN–LAUB model is distinct from the others. However, it can be seen that $\boldsymbol{f}_I^{\mathrm{EL}} = \boldsymbol{f}_I^{\mathrm{A}_2} - \frac{1}{6}\mu_0 M_0^2 \boldsymbol{e}_r$; hence, these models only differ by a constant radial (pressure) offset. Qualitative representations of the surface force densities are shown in Fig. 9.

Furthermore, one can note that all models with a non-symmetric stress measure yield purely radial surface force densities in this problem. Interestingly, whereas the radial force components of the non-symmetric models attain their maxima at the poles, the symmetric models attain them at the equator. The maxima of the surface force norm, divided by $\mu_0 M_0^2$, read

$$\max_{\vartheta\in[0,\pi/2]} \|\tilde{\boldsymbol{f}}_I^{(1)}\| = \frac{4}{3\sqrt{15}} \approx 0.34, \quad \max_{\vartheta\in[0,\pi/2]} \|\tilde{\boldsymbol{f}}_I^{(2)}\| = \frac{2}{3}, \quad \max_{\vartheta\in[0,\pi/2]} \|\tilde{\boldsymbol{f}}_I^{(3)}\| = \frac{1}{2}.$$

6.2 Magnetostriction effects

Note that all considered electromagnetic force models yield vanishing volumetric force densities and only surface densities remain. For this problem, gravitational body forces can be neglected. Then the balance of linear momentum in regular points reduces and reads $\nabla \cdot \boldsymbol{\sigma} = \mathbf{0}$, where $\boldsymbol{\sigma}$ is the *mechanical* stress tensor. For linear elasticity with small deformations and isotropic media, HOOKE's law in the form

$$\boldsymbol{\sigma} = \lambda(\nabla \cdot \boldsymbol{u})\mathbf{1} + \mu(\nabla \otimes \boldsymbol{u} + \boldsymbol{u} \otimes \nabla)$$

can be employed. Here, $\boldsymbol{u}$ is the displacement field and λ, μ denote LAMÉ's parameters. Note that it is assumed that the mechanical stress has no *direct* dependency on the electromagnetic fields. Of course, the stress is indirectly influenced by the electromagnetic fields due to the electromagnetic force distributions. If the considered material possesses a direct dependency upon the electromagnetic fields, then there would be too many unknowns. In this case, both the mechanical stress tensor and the electromagnetic force model need to be determined simultaneously via experiments, which is not possible.

Insertion of the HOOKE's law into the momentum equation yields the homogeneous LAMÉ–NAVIER equations,

$$(\lambda + \mu)\nabla(\nabla \cdot \boldsymbol{u}) + \mu \Delta \boldsymbol{u} = \mathbf{0}.$$

For problems with spherical geometry and azimuthal symmetry, these equations were solved in a general manner by HIRAMATSU and OKA, *cf.* [14]. Their solution for the displacements (and therefore also for the stresses) is given by means of series containing powers of the spherical radial coordinate and LEGENDRE polynomials,

$$u_r(\tilde{r}, \vartheta) = R \sum_{n=0}^{\infty} \left[-\frac{n\frac{\lambda}{\mu} + n - 2}{2(2n+3)} A_n \tilde{r}^{n+1} + n B_n \tilde{r}^{n-1} \right] P_n(x),$$
$$u_\vartheta(\tilde{r}, \vartheta) = R \sum_{n=1}^{\infty} \left[-\frac{(n+3)\frac{\lambda}{\mu} + n + 5}{2(n+1)(2n+3)} A_n \tilde{r}^{n+1} + B_n \tilde{r}^{n-1} \right] \frac{\mathrm{d}P_n(x)}{\mathrm{d}\vartheta},$$

in which $P_n(x)$ denotes the nth LEGENDRE polynomial. We assume that there is no relevant pressure outside the sphere so that $\boldsymbol{\sigma}^{\text{ext}} = \mathbf{0}$. The jump condition of linear momentum for this scenario, Eq. (B.4), reads for any electromagnetic force model

$$\boldsymbol{n} \cdot [\![\boldsymbol{\sigma}]\!] = -\boldsymbol{f}_l^{(\text{EM})} \quad \Rightarrow \quad \boldsymbol{n} \cdot \boldsymbol{\sigma} = \boldsymbol{f}_l^{(\text{EM})}.$$

Due to azimuthal symmetry, we can decompose the force densities to read

$$\boldsymbol{f}_l^{(\text{EM})} = f_r^{(\text{EM})} \boldsymbol{e}_r + f_\vartheta^{(\text{EM})} \boldsymbol{e}_\vartheta.$$

Hence, the jump equation yields two (non-trivial) relations. With $\sigma_{rr} = \boldsymbol{e}_r \cdot \boldsymbol{\sigma} \cdot \boldsymbol{e}_r$ and $\sigma_{r\vartheta} = \boldsymbol{e}_r \cdot \boldsymbol{\sigma} \cdot \boldsymbol{e}_\vartheta$, they read

$$\sigma_{rr}(\tilde{r} = 1, \vartheta) = f_r^{(\text{EM})}(\vartheta), \quad \sigma_{r\vartheta}(\tilde{r} = 1, \vartheta) = f_\vartheta^{(\text{EM})}(\vartheta).$$

By inserting the series solution of the displacements, one finds that σ_{rr} depends upon the LEGENDRE polynomials $P_n(x)$. Furthermore, one can see that the shear stress $\sigma_{r\vartheta}$ depends upon derivatives of these polynomials, $\mathrm{d}P_n(x)/\mathrm{d}\vartheta$. As demonstrated in [30], an expansion of $f_r^{(\text{EM})}$ w.r.t. $P_n(x)$ and $f_\vartheta^{(\text{EM})}$ w.r.t. $\mathrm{d}P_n(x)/\mathrm{d}\vartheta$ is convenient. The expansions of the obtained force densities read

$$\boldsymbol{f}_l^{(1)}(x) = \mu_0 M_0^2 ([\tfrac{1}{9} P_0(x) - \tfrac{1}{9} P_2(x)]\boldsymbol{e}_r - \tfrac{2}{9} \tfrac{\mathrm{d}P_2(x)}{\mathrm{d}\vartheta} \boldsymbol{e}_\vartheta),$$
$$\boldsymbol{f}_l^{(2)}(x) = \mu_0 M_0^2 [\tfrac{1}{3} P_0(x) + \tfrac{1}{3} P_2(x)]\boldsymbol{e}_r,$$
$$\boldsymbol{f}_l^{(3)}(x) = \mu_0 M_0^2 [\tfrac{1}{6} P_0(x) + \tfrac{1}{3} P_2(x)]\boldsymbol{e}_r.$$

Then, with the relations of orthogonality of the LEGENDRE polynomials, the coefficients A_n and B_n are readily obtained; see [30]. Only a few obtained series coefficients are non-trivial; hence, the series degenerates to a

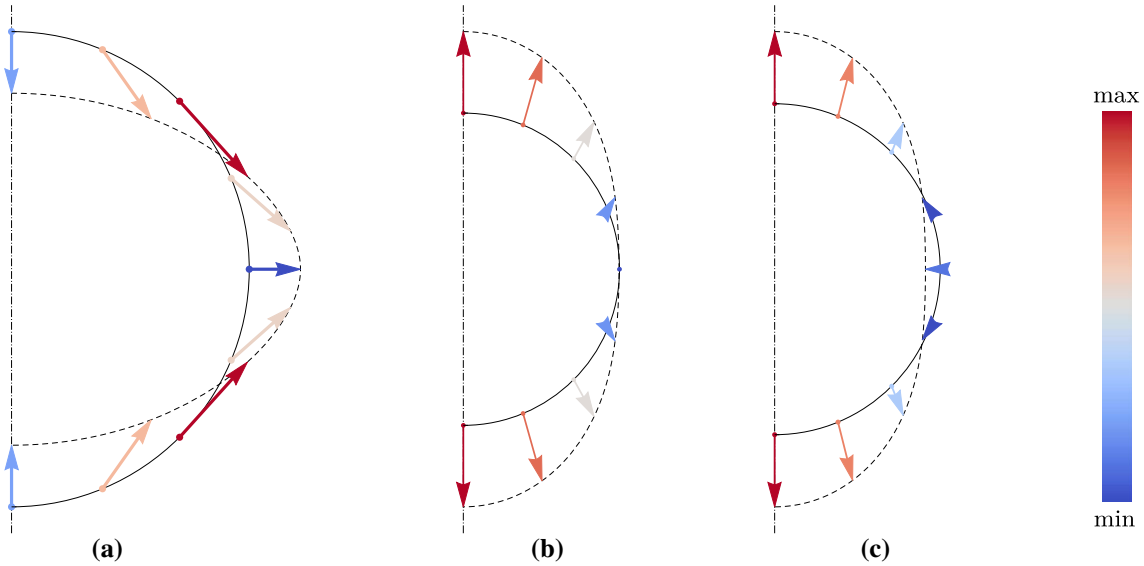

Fig. 10 Qualitative visualization of the surface displacements for the three electromagnetic force results. The ratio $\lambda/\mu = 1.27$ was used in order to model steel. **a** $\boldsymbol{u}^{(1)}$. **b** $\boldsymbol{u}^{(2)}$. **c** $\boldsymbol{u}^{(3)}$

finite sum. By using the normalization $A_j^i = \frac{\mu_0 M_0^2}{\mu} \hat{A}_j^{(i)}$, and analogously for $B_j^{(i)}$, the non-trivial coefficients are obtained as

$$\hat{A}_0^{(1)} = \frac{1}{6+9\frac{\lambda}{\mu}}, \qquad \hat{A}_2^{(1)} = \frac{7}{14+19\frac{\lambda}{\mu}}, \qquad \hat{B}_2^{(1)} = -\frac{7}{18}\frac{1+2\frac{\lambda}{\mu}}{14+19\frac{\lambda}{\mu}},$$

$$\hat{A}_0^{(2)} = \frac{1}{2+3\frac{\lambda}{\mu}}, \qquad \hat{A}_2^{(2)} = \frac{7}{14+19\frac{\lambda}{\mu}}, \qquad \hat{B}_2^{(2)} = \frac{1}{6}\frac{7+8\frac{\lambda}{\mu}}{14+19\frac{\lambda}{\mu}},$$

$$\hat{A}_0^{(3)} = \frac{1}{4+6\frac{\lambda}{\mu}}, \qquad \hat{A}_2^{(3)} = \frac{7}{14+19\frac{\lambda}{\mu}}, \qquad \hat{B}_2^{(3)} = \frac{1}{6}\frac{7+8\frac{\lambda}{\mu}}{14+19\frac{\lambda}{\mu}}.$$

As the series degenerate, closed-form displacement solutions are obtained. The displacement results for the three models are depicted in Fig. 10.

From the figure, one can see that all force models result in a (differently) deformed spheroid. Note that the poles flatten for the symmetric models, *i.e.*, the displacement is negative there. In contrast to that, the displacements of the other results are positive at the poles. At the equator, the displacements are distinct for all three solutions. In the first result, one can observe that the two equal half axes increase in length. For the second result, no measurable displacement can be observed. In the third result, the equatorial half axes shrink visibly. In order to ensure that this does not depend upon the chosen value $\lambda/\mu = 1.27$ in the visualization of Fig. 10, the ratio $u_r(\tilde{r} = 1, \vartheta = \frac{\pi}{2})/u_r(\tilde{r} = 1, \vartheta = 0)$ is analyzed. Noting that $\frac{\lambda}{\mu} = \frac{2\nu}{1-2\nu}$, this displacement ratio is plotted over a range of common values for POISSON's ratio ν for metals in Fig. 11. One can see that for realistic values of ν the equatorial displacement is negligibly small in the second result.

6.3 Discussion of the results

In conclusion, the first solution yields an oblate spheriod, the other two prolate spheroids. The two prolate spheroids can be distinguished by measuring the equatorial displacement—one solution shows no measurable equatorial displacement, whereas the other yields a negative equatorial displacement. This difference may be explained by the fact that the two forces differ by a constant radial force.

All resulting displacements are small. First, one can note that the dimensionless amplifying functions of the displacements are of order 10^{-1} for all models. As an example, consider a spherical magnet with

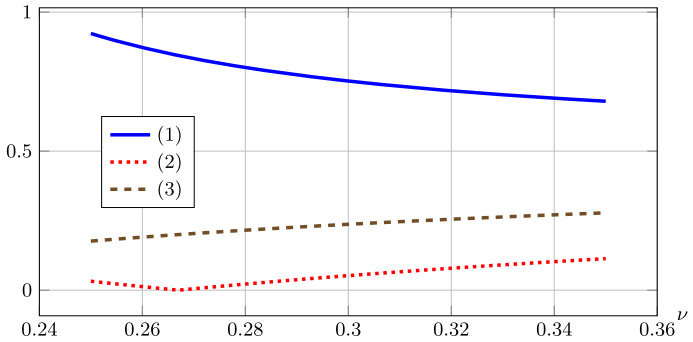

Fig. 11 The displacement ratio $u_r(\tilde{r} = 1, \vartheta = \frac{\pi}{2})/u_r(\tilde{r} = 1, \vartheta = 0)$ for the three force results. This ratio is plotted against POISSON's ratio in a common range of metals

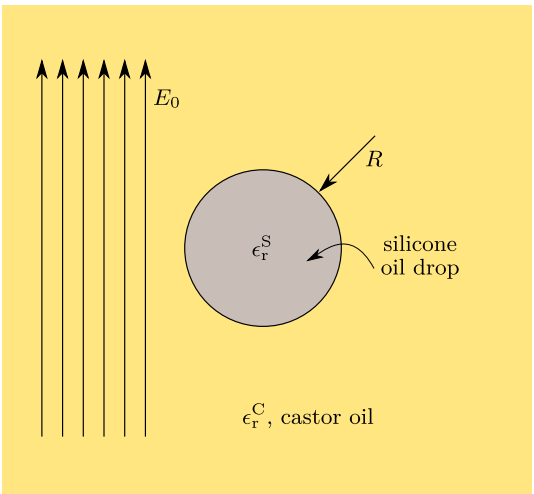

Fig. 12 A silicone oil drop in castor oil. The experiment is placed in an external homogeneous static electric field

$R = 10\,\text{mm}$, $\mu_0 M_0 = 1\,\text{T}$ and $\mu = 80\,\text{GPa}$. Then, the amplitude of the displacements for this scenario is $\|\boldsymbol{u}\| = \frac{\mu_0 M_0^2}{\mu} \|\tilde{\boldsymbol{u}}\| R \approx 10\,\text{nm}$. Other geometries and remanences do not significantly change the obtained displacement scale. Therefore, in order to (in)validate certain force models, high-precision measuring instruments are required. Note that the scale of the displacements can be increased, if a linear-magnetic sphere is placed in an external magnetic field; see [30].

7 Another example of local effects: a drop of silicone oil in castor oil

Another example to demonstrate local effects of the force models is the examination of a spherical silicone oil drop of radius R in oxidized castor oil, placed in an homogeneous electric field $\boldsymbol{E}_0 = E_0 \boldsymbol{e}_z$. This experiment was conducted in [38]. We assume linear polarization laws with the relative dielectric constants of silicone oil $\epsilon_r^S \approx 2.8$ and of castor oil $\epsilon_r^C \approx 6.3$. The values are taken from an experiment in [38, Table. 1, system 16]. Also, the densities of the oils are nearly equal. Hence, gravitational effects can be neglected. The experiment is sketched in Fig. 12.

The results of the experiments conducted in [38] recently motivated [7] to compare force models. In contrast to the demonstrated problem of magnetostriction, the deformations in this experiment can be large, depending on the external field strength, and are clearly observable. The authors of [7] computed the forces for different models, and their force results can be classified in two groups. In the first group, there are no forces at the poles and large pressure forces at the equator. In the second group, there are pressure forces at the poles and no forces at the equator. As the conducted experiment of [38] shows a prolate spheroid with an applied electric field, they dismissed the models corresponding to the first group—this is a reasonable conclusion. For the second group,

they compared the calculated force distributions to the deformation figure of the experimental photographs of [38]. They refrained from actually computing the surface deformations. From the force distribution alone, they argued that a "LORENTZ" tensor of the form

$$\boldsymbol{\sigma}^{\mathrm{L,alt}} = -\tfrac{1}{2}(\epsilon_0 \boldsymbol{E}\cdot\boldsymbol{E} + \mu_0 \mathfrak{H}\cdot\mathfrak{H})\mathbf{1} + \epsilon_0 \boldsymbol{E}\otimes\boldsymbol{E} + \mu_0 \mathfrak{H}\otimes\mathfrak{H},$$

predicts the experiment well.

However, the mechanics is more complicated, even in the static case. The oils do not mix, *i.e.*, there is some mechanical surface stress that balances the electromagnetic forces. It is not immediately clear how the forces correspond to the displacement figure. Therefore, an attempt is made here to model the surface stress in order to calculate the resulting deformation figure. As with magnetostriction, we restrict the calculations to small deformations, *i.e.*, a small applied electric field strength. Then, the predicted displacements can be compared with experimental photographs of [38] and reliable conclusions can be drawn.

First, we briefly solve the electric problem and proceed with the computation of the resulting force densities for the previously discussed models in this work. Then, surface stresses and deformations are investigated. The displacements are computed for all force models and compared to experimental results from [38].

7.1 Electric field computation

Due to the linearity of MAXWELL's equations, the electric field can be decomposed as $\boldsymbol{E} = \boldsymbol{E}_0 + \boldsymbol{E}^{\mathrm{dist.}}$, where the external field $\boldsymbol{E}_0$ is homogeneous. Then, FARADAY's law of induction in Table 2 reduces to

$$\nabla\times\boldsymbol{E}^{\mathrm{dist.}} = \mathbf{0}, \quad \boldsymbol{n}\times[\![\boldsymbol{E}^{\mathrm{dist.}}]\!] = \mathbf{0}, \quad \text{which is solved by} \quad \boldsymbol{E}^{\mathrm{dist.}} = -\nabla V, \quad [\![V]\!] = 0.$$

Scaling the lengths in the system by R and the distortion potential by $E_0 R$, so that $V = E_0 R\mathcal{V}$ and $\nabla = \frac{1}{R}\tilde{\nabla}$, the above is equal to

$$\boldsymbol{E} = E_0(\boldsymbol{e}_z - \tilde{\nabla}\mathcal{V}), \quad [\![\mathcal{V}]\!] = 0.$$

Denoting $\mathcal{V}^{\mathrm{S}}$ for the potential function in the silicone drop, and $\mathcal{V}^{\mathrm{C}}$ for the function in the exterior castor oil domain, the polarizations and the free charge potentials read

$$\boldsymbol{P}^{\mathrm{S}} = \epsilon_0(\epsilon_{\mathrm{r}}^{\mathrm{S}} - 1)\boldsymbol{E}^{\mathrm{S}} = E_0\epsilon_0(\epsilon_{\mathrm{r}}^{\mathrm{S}} - 1)(\boldsymbol{e}_z - \tilde{\nabla}\mathcal{V}^{\mathrm{S}}), \quad \boldsymbol{P}^{\mathrm{C}} = \epsilon_0(\epsilon_{\mathrm{r}}^{\mathrm{C}} - 1)\boldsymbol{E}^{\mathrm{C}} = E_0\epsilon_0(\epsilon_{\mathrm{r}}^{\mathrm{C}} - 1)(\boldsymbol{e}_z - \tilde{\nabla}\mathcal{V}^{\mathrm{C}}),$$
$$\mathfrak{D}^{\mathrm{S}} = \epsilon_0\epsilon_{\mathrm{r}}^{\mathrm{S}}\boldsymbol{E}^{\mathrm{S}} = E_0\epsilon_0\epsilon_{\mathrm{r}}^{\mathrm{S}}(\boldsymbol{e}_z - \tilde{\nabla}\mathcal{V}^{\mathrm{S}}), \quad \mathfrak{D}^{\mathrm{C}} = \epsilon_0\epsilon_{\mathrm{r}}^{\mathrm{C}}\boldsymbol{E}^{\mathrm{C}} = E_0\epsilon_0\epsilon_{\mathrm{r}}^{\mathrm{C}}(\boldsymbol{e}_z - \tilde{\nabla}\mathcal{V}^{\mathrm{C}}).$$

Since the free macroscopic charge density vanishes in the problem, the free charge potentials are solenoidal. Therefore, both $\mathcal{V}^{\mathrm{S}}$ and $\mathcal{V}^{\mathrm{C}}$ satisfy the LAPLACE equation, *i.e.*,

$$\tilde{\Delta}\mathcal{V}^{\mathrm{S}} = 0, \quad \text{and} \quad \tilde{\Delta}\mathcal{V}^{\mathrm{C}} = 0.$$

The solutions of these LAPLACE problems with azimuthal symmetry that satisfy conditions of integrability and finiteness read

$$\mathcal{V}^{\mathrm{S}} = \sum_{n=0}^{\infty} a_n \tilde{r}^n P_n(x), \quad \mathcal{V}^{\mathrm{C}} = \sum_{n=0}^{\infty} b_n \tilde{r}^{-(n+1)} P_n(x),$$

where $x = \cos\vartheta$, $\tilde{r} = r/R$, and P_n denote LEGENDRE polynomials. It is easy to see that the condition of continuity, $[\![\mathcal{V}]\!] = 0$, is satisfied by setting $a_n = b_n$. The second transition condition, with $\boldsymbol{n} = \boldsymbol{e}_r$ and $\cos\vartheta = P_1(x)$, reads

$$\boldsymbol{n}\cdot[\![\mathfrak{D}]\!] = 0 \quad \Leftrightarrow \quad \epsilon_{\mathrm{r}}^{\mathrm{C}}\frac{\partial\mathcal{V}^{\mathrm{C}}}{\partial\tilde{r}} - \epsilon_{\mathrm{r}}^{\mathrm{S}}\frac{\partial\mathcal{V}^{\mathrm{S}}}{\partial\tilde{r}} = (\epsilon_{\mathrm{r}}^{\mathrm{C}} - \epsilon_{\mathrm{r}}^{\mathrm{S}})P_1(x).$$

One finds that

$$a_1 = b_1 = -\frac{\epsilon_{\mathrm{r}}^{\mathrm{C}} - \epsilon_{\mathrm{r}}^{\mathrm{S}}}{2\epsilon_{\mathrm{r}}^{\mathrm{C}} + \epsilon_{\mathrm{r}}^{\mathrm{S}}},$$

and all other coefficients are zero. The series degenerates and the distortion potentials are

$$\mathcal{V}^{\mathrm{S}} = -\frac{\epsilon_{\mathrm{r}}^{\mathrm{C}} - \epsilon_{\mathrm{r}}^{\mathrm{S}}}{2\epsilon_{\mathrm{r}}^{\mathrm{C}} + \epsilon_{\mathrm{r}}^{\mathrm{S}}}\tilde{r}\cos\vartheta, \quad \mathcal{V}^{\mathrm{C}} = -\frac{\epsilon_{\mathrm{r}}^{\mathrm{C}} - \epsilon_{\mathrm{r}}^{\mathrm{S}}}{2\epsilon_{\mathrm{r}}^{\mathrm{C}} + \epsilon_{\mathrm{r}}^{\mathrm{S}}}\tilde{r}^{-2}\cos\vartheta.$$

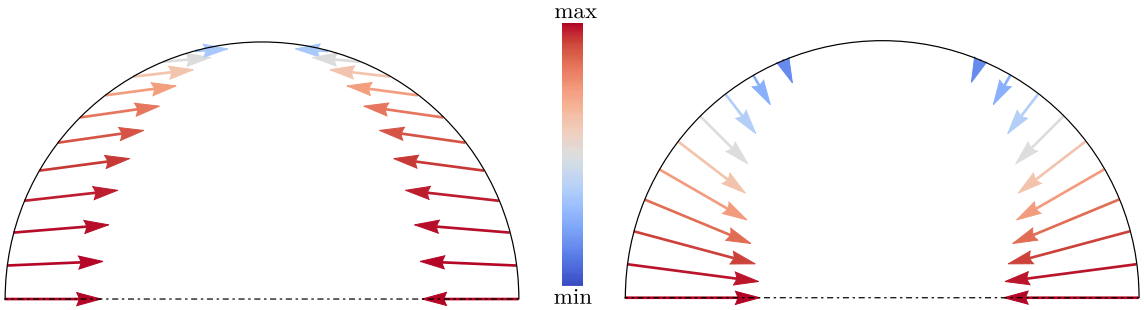

Fig. 13 Qualitative representation of the computed force results for the oil drop experiment. For visualization, the values $\epsilon_{\mathrm{r}}^{\mathrm{S}} = 2.8$ and $\epsilon_{\mathrm{r}}^{\mathrm{C}} = 6.3$ are employed. Note that the external electric field is in the horizontal direction. **a** Surface force $\boldsymbol{f}_I^{(4)}$. **b** Surface force $\boldsymbol{f}_I^{(5)}$

7.2 Force densities

Through an analogous investigation of the force models as for the spherical magnetostriction problem, one finds that the volumetric force density vanishes for every considered model. Furthermore, one obtains for the surface densities that

$$\begin{aligned}
\boldsymbol{f}_I^{(4)} &= \boldsymbol{f}_I^{\mathrm{L}} = \boldsymbol{f}_I^{\mathrm{A}_1} = \boldsymbol{f}_I^{\mathrm{A}_2} = \boldsymbol{f}_I^{\mathrm{M}_1} = -(\boldsymbol{n} \cdot [\![\boldsymbol{P}]\!])\langle \boldsymbol{E} \rangle \\
&= -\tfrac{9}{2}\epsilon_0 E_0^2 \tfrac{\epsilon_{\mathrm{r}}^{\mathrm{C}} - \epsilon_{\mathrm{r}}^{\mathrm{S}}}{(2\epsilon_{\mathrm{r}}^{\mathrm{C}} + \epsilon_{\mathrm{r}}^{\mathrm{S}})^2} [(\epsilon_{\mathrm{r}}^{\mathrm{C}} + \epsilon_{\mathrm{r}}^{\mathrm{S}}) \cos^2\vartheta \boldsymbol{e}_r - 2\epsilon_{\mathrm{r}}^{\mathrm{C}} \cos\vartheta \sin\vartheta \boldsymbol{e}_\vartheta], \\
\boldsymbol{f}_I^{(5)} &= \boldsymbol{f}_I^{\mathrm{M}_2} = \boldsymbol{f}_I^{\mathrm{EL}} = \boldsymbol{n}(\langle \boldsymbol{P} \rangle \cdot [\![\boldsymbol{E}]\!]) = -\tfrac{9}{2}\epsilon_0 E_0^2 \tfrac{\epsilon_{\mathrm{r}}^{\mathrm{C}} - \epsilon_{\mathrm{r}}^{\mathrm{S}}}{(2\epsilon_{\mathrm{r}}^{\mathrm{C}} + \epsilon_{\mathrm{r}}^{\mathrm{S}})^2} (2\epsilon_{\mathrm{r}}^{\mathrm{C}} \epsilon_{\mathrm{r}}^{\mathrm{S}} - \epsilon_{\mathrm{r}}^{\mathrm{C}} - \epsilon_{\mathrm{r}}^{\mathrm{S}}) \cos^2\vartheta \boldsymbol{e}_r.
\end{aligned}$$

As before, one result shows shear as well as normal stresses, whereas the other yields pure normal stresses. The force results are depicted in Fig. 13.

7.3 Surface deformation

In order to gain insight as to which force model(s) concur with experiments, the mechanical surface stress tensor has to be modeled. Before an electric field is activated, it can be assumed that the spherical drop is subjected to a purely tension dependent surface stress of the form

$$\boldsymbol{\sigma}_I^0 = \sigma_I \mathbf{1}_I, \quad \mathbf{1}_I = \mathbf{1} - \boldsymbol{e}_r \otimes \boldsymbol{e}_r.$$

Here, σ_I is the surface tension between the two oils. As the two oils are at rest, the volumetric stresses are given by

$$\boldsymbol{\sigma}^{\mathrm{C}} = -p^{\mathrm{C}}\mathbf{1}, \quad \boldsymbol{\sigma}_0^{\mathrm{S}} = -p_0^{\mathrm{S}}\mathbf{1}.$$

Notation wise, the pressure of the castor oil is not given an extra index for the unloaded situation as it can be assumed that this pressure will remain constant. For this initial state, the balance of momentum for interfaces in Eq. (B.3) reads

$$-\boldsymbol{\sigma}_I \cdot \nabla_I = [\![\boldsymbol{\sigma}]\!] \cdot \boldsymbol{n} \quad \Rightarrow \quad p_0^{\mathrm{S}} = p^{\mathrm{C}} + \tfrac{2\sigma_I}{R},$$

where R is the radius of the sphere in this initial state. Here, it is assumed that the interface does not carry mass, *i.e.*, $\rho_I = 0$. This result for the pressure jump is well-known in the literature, *e.g.*, [26, Sect. 7.2]. If an electric field is applied, a model-dependent force density acts on the sphere. From experiments it is known that small electric fields do not cause the droplet to burst. However, it deforms. As the deformation is bounded, there must be some kind of mechanical reaction that balances the electromagnetic force. We shall assume that the interface of the two oils possesses isotropic elastic behavior and state the surface stress in the form

$$\boldsymbol{\sigma}_I = (\sigma_I + \lambda_I \boldsymbol{\varepsilon}_I \cdot\cdot\, \mathbf{1}_I)\mathbf{1}_I + 2\mu_I \boldsymbol{\varepsilon}_I, \quad \boldsymbol{\varepsilon}_I = \mathbf{1}_I \cdot \tfrac{1}{2}(\boldsymbol{u}_I \otimes \nabla_I + \nabla_I \otimes \boldsymbol{u}_I) \cdot \mathbf{1}_I,$$

motived by relations given in [19,32]. Here, $\boldsymbol{u}_I$ is the surface displacement field. Note that analogously to the magnetostriction problem, no direct dependency of the mechanical stress on the electromagnetic fields is assumed. The following analysis is restricted to small deformations only. This is sufficient to gain insight into the nature of the resulting deformation figure. Hence, variables and base vectors of the initial and of the current placement of the droplet are not distinguished here. Due to azimuthal symmetry of the loading, the surface displacement is of the form

$$\boldsymbol{u}_I = \hat{u}(\tilde{u}_r(\vartheta)\boldsymbol{e}_r + \tilde{u}_\vartheta(\vartheta)\boldsymbol{e}_\vartheta),$$

where $\hat{u}$ contains the scale and dimension of the displacement field. The forces are also stated in scaled form,

$$\boldsymbol{f}_I^{(\mathrm{EM})} = \hat{f}(f_r(\vartheta)\boldsymbol{e}_r + f_\vartheta(\vartheta)\boldsymbol{e}_\vartheta), \quad \hat{f} = \tfrac{9}{2}\epsilon_0 E_0^2 \tfrac{\epsilon_\mathrm{r}^\mathrm{C}-\epsilon_\mathrm{r}^\mathrm{S}}{(2\epsilon_\mathrm{r}^\mathrm{C}+\epsilon_\mathrm{r}^\mathrm{S})^2}.$$

The scale $\hat{f}$ is a common factor of the densities $\boldsymbol{f}_I^{(4)}$ and $\boldsymbol{f}_I^{(5)}$. However, the functions f_r and f_ϑ must be taken from the analyzed force result. Independently of the applied force model, the divergence of the surface stress is as follows:

$$\begin{aligned}\boldsymbol{\sigma}_I \cdot \nabla_I = &-2\tfrac{\mu_I}{R}\tfrac{\hat{u}}{R}[\tfrac{R\sigma_I}{\hat{u}\mu_I} + 2(1+\tfrac{\lambda_I}{\mu_I})\{\tilde{u}_r + \cot\vartheta\,\tilde{u}_\vartheta + \tilde{u}'_\vartheta\}]\boldsymbol{e}_r \\ &+\tfrac{\mu_I}{R}\tfrac{\hat{u}}{R}[-(1+\tfrac{\lambda_I}{\mu_I}+\cos 2\vartheta)\csc^2\vartheta\,\tilde{u}_\vartheta + 2(1+\tfrac{\lambda_I}{\mu_I})\tilde{u}'_r + (2+\tfrac{\lambda_I}{\mu_I})\{\cot\vartheta\,\tilde{u}'_\vartheta + \tilde{u}''_\vartheta\}]\boldsymbol{e}_\vartheta.\end{aligned}$$

It is used in the singular balance of momentum containing electromagnetic surface forces, *i.e.*,

$$\boldsymbol{\sigma}_I \cdot \nabla_I + [\![\boldsymbol{\sigma}]\!] \cdot \boldsymbol{n} + \boldsymbol{f}_I^{(\mathrm{EM})} = \boldsymbol{0}.$$

This vector equation yields two linearly independent component equations, *viz.*

$$-2\tfrac{\mu_I}{R}\tfrac{\hat{u}}{R}[\tfrac{\sigma_I R}{\hat{u}\mu_I} + (1+\tfrac{\lambda_I}{\mu_I})\{2\tilde{u}_r + \cot\vartheta\,\tilde{u}_\vartheta + \tilde{u}'_\vartheta\}] + p^\mathrm{S} - p^\mathrm{C} + \hat{f} f_r = 0, \tag{7.1a}$$

$$\tfrac{\mu_I}{R}\tfrac{\hat{u}}{R}[2(1+\tfrac{\lambda_I}{\mu_I})\tilde{u}'_r - (1+\tfrac{\lambda_I}{\mu_I}+\cos 2\vartheta)\csc^2\vartheta\,\tilde{u}_\vartheta + (2+\tfrac{\lambda_I}{\mu_I})\{\cot\vartheta\,\tilde{u}'_\vartheta + \tilde{u}''_\vartheta\}] + \hat{f} f_\vartheta = 0. \tag{7.1b}$$

It is helpful to take the derivative w.r.t. ϑ of Eq. (7.1a), yielding

$$-2\tfrac{\mu_I}{\hat{f}R}\tfrac{\hat{u}}{R}(1+\tfrac{\lambda_I}{\mu_I})\{2\tilde{u}'_r - \csc^2\vartheta\,\tilde{u}_\vartheta + \cot\vartheta\,\tilde{u}'_\vartheta + \tilde{u}''_\vartheta\} + f'_r = 0. \tag{7.2}$$

This equation and also Eq. (7.1b) motivate the choice of displacement scale,

$$\hat{u} = \tfrac{\hat{f}R}{\mu_I}R,$$

so that Eqs. (7.2) and (7.1b) simplify to

$$-2(1+\tfrac{\lambda_I}{\mu_I})\{2\tilde{u}'_r - \csc^2\vartheta\,\tilde{u}_\vartheta + \cot\vartheta\,\tilde{u}'_\vartheta + \tilde{u}''_\vartheta\} + f'_r = 0, \tag{7.3a}$$

$$2(1+\tfrac{\lambda_I}{\mu_I})\tilde{u}'_r - (1+\tfrac{\lambda_I}{\mu_I}+\cos 2\vartheta)\csc^2\vartheta\,\tilde{u}_\vartheta + (2+\tfrac{\lambda_I}{\mu_I})\{\cot\vartheta\,\tilde{u}'_\vartheta + \tilde{u}''_\vartheta\} + f_\vartheta = 0. \tag{7.3b}$$

Both equations contain the radial displacement only in form of $\tilde{u}'_r$, and hence, it can be eliminated; this yields

$$-2[(1-\cot^2\vartheta)\tilde{u}_\vartheta + \cot\vartheta\,\tilde{u}'_\vartheta + \tilde{u}''_\vartheta] = 2f_\vartheta + f'_r. \tag{7.4}$$

Remarkably, this relation does not depend upon the elastic moduli. From symmetry of the analyzed forces, one has $\tilde{u}_\vartheta(\vartheta = 0) = \tilde{u}_\vartheta(\vartheta = \pi/2) = 0$. The right-hand side of Eq. (7.4) is a given function of the force model. Hence, this equation can be solved for the function $\tilde{u}_\vartheta$, depending on the force model. As the current pressure in the silicone oil is unknown, Eq. (7.1a) cannot be used directly to obtain $\tilde{u}_r$. Rather, Eq. (7.3a) is to be used. At this point, $\tilde{u}_\vartheta$ is a known function, and hence, Eq. (7.3a) is an ordinary differential equation for $\tilde{u}_r$. However, for this function, there is no symmetry argument available in order to obtain a functional value at any point. The (unknown) displacement of the pole is introduced as a parameter by setting $\tilde{u}_\mathrm{P} := \tilde{u}_r(\vartheta = 0)$ instead. The equation is consequently solved by using this parameter. From the previously computed forces, one can assume that this parameter is negative, *i.e.*, an oblate deformation occurs. In order to obtain $\tilde{u}_\mathrm{P}$, a constitutive relation is needed for the pressure of the silicone oil drop. This oil is compressible, the relation

between pressure and relative volume change is in general nonlinear. However, as only small deformations are regarded, it is reasonable to employ a linear relationship,

$$p^{\mathrm{S}} = p_0^{\mathrm{S}}(1+\chi_{\mathrm{v}}^{\mathrm{S}} e_{\mathrm{v}}^{\mathrm{S}}) = (p^{\mathrm{C}} + \tfrac{2\sigma_I}{R})(1+\chi_{\mathrm{v}}^{\mathrm{S}} e_{\mathrm{v}}^{\mathrm{S}}), \quad e_{\mathrm{v}}^{\mathrm{S}} = \tfrac{V_0^{\mathrm{S}} - V^{\mathrm{S}}}{V_0^{\mathrm{S}}},$$

where V_0^{S} and V^{S} are the volumes of the oil drop in the undeformed and deformed state, respectively. Here, one can denote

$$V_0^{\mathrm{S}} = \tfrac{4}{3}\pi R^3 = \frac{R}{3}\oint\limits_{\partial\Omega_0^{\mathrm{S}}} \boldsymbol{e}_r \cdot \mathrm{d}\boldsymbol{A}_0, \quad V^{\mathrm{S}} = \int\limits_{\Omega^{\mathrm{S}}} \mathrm{d}V = \frac{1}{3}\int\limits_{\Omega^{\mathrm{S}}} \boldsymbol{x}\cdot\nabla \mathrm{d}V = \frac{1}{3}\oint\limits_{\partial\Omega^{\mathrm{S}}} \boldsymbol{x}\cdot\mathrm{d}\boldsymbol{A} = \frac{1}{3}\oint\limits_{\partial\Omega_0^{\mathrm{S}}} (\boldsymbol{X}+\boldsymbol{u})\cdot \boldsymbol{J}\boldsymbol{F}^{-\mathrm{T}}\cdot \mathrm{d}\boldsymbol{A}_0.$$

As the integrand does not possess azimuthal dependency after projection, one can write

$$\mathrm{d}\boldsymbol{A}_0 = \boldsymbol{e}_r 2\pi R^2 \sin\vartheta \,\mathrm{d}\vartheta.$$

Formally, one obtains

$$e_{\mathrm{v}}^{\mathrm{S}} = \frac{1}{2R}\int\limits_{\vartheta=0}^{\pi} [R - (\boldsymbol{X}+\boldsymbol{u})\cdot \boldsymbol{J}\boldsymbol{F}^{-\mathrm{T}}\cdot \boldsymbol{e}_R]\sin\vartheta \;\mathrm{d}\vartheta.$$

It is convenient to linearize this relation, applicable for small volume changes. One obtains that

$$e_{\mathrm{v}}^{\mathrm{S}} \approx -\frac{1}{2}\frac{\hat{u}}{R}\int\limits_{\vartheta=0}^{\pi} [3\tilde{u}_r + \cot\vartheta\,\tilde{u}_\vartheta + \tilde{u}'_\vartheta]\sin\vartheta \;\mathrm{d}\vartheta = \tfrac{\hat{f}R}{\mu_I}\tilde{e}_{\mathrm{v}}^{\mathrm{S}}.$$

This value can be computed symbolically, still containing the unknown factor $\tilde{u}_{\mathrm{P}}$. The pressure jump then reads

$$p^{\mathrm{S}} - p^{\mathrm{C}} = (p^{\mathrm{C}} + \tfrac{2\sigma_I}{R})(1+\chi_{\mathrm{v}}^{\mathrm{S}} e_{\mathrm{v}}^{\mathrm{S}}) - p^{\mathrm{C}} = p^{\mathrm{C}}\chi_{\mathrm{v}}^{\mathrm{S}} e_{\mathrm{v}}^{\mathrm{S}} + \tfrac{2\sigma_I}{R}(1+\chi_{\mathrm{v}}^{\mathrm{S}} e_{\mathrm{v}}^{\mathrm{S}}).$$

Insertion of this relation with the previously chosen displacement scale in Eq. (7.1a) shows that

$$-2(1+\tfrac{\lambda_I}{\mu_I})\{2\tilde{u}_r + \cot\vartheta\,\tilde{u}_\vartheta + \tilde{u}'_\vartheta\} + \gamma\tilde{e}_{\mathrm{v}}^{\mathrm{S}} + f_r = 0, \quad \gamma := (\tfrac{p^{\mathrm{C}}R}{\mu_I} + \tfrac{2\sigma_I}{\mu_I})\chi_{\mathrm{v}}^{\mathrm{S}} = \tfrac{p_0^{\mathrm{S}}R}{\mu_I}\chi_{\mathrm{v}}^{\mathrm{S}}.$$

From this equation, $\tilde{u}_{\mathrm{P}}$ follows and the problem is formally solved.

Computation with $\boldsymbol{f}_I^{(4)}$, where the force functions are given by

$$f_r^{(4)} = -(\epsilon_{\mathrm{r}}^{\mathrm{C}} + \epsilon_{\mathrm{r}}^{\mathrm{S}})\cos^2\vartheta, \quad f_\vartheta^{(4)} = \epsilon_{\mathrm{r}}^{\mathrm{C}}\sin 2\vartheta.$$

By using these, the polar displacement follows as

$$\tilde{u}_\vartheta^{(4)} = \tfrac{1}{8}(3\epsilon_{\mathrm{r}}^{\mathrm{C}} + \epsilon_{\mathrm{r}}^{\mathrm{S}})\sin 2\vartheta,$$

and, by using this result, the radial displacement reads

$$\tilde{u}_r^{(4)} = \tilde{u}_{\mathrm{P}}^4 + (16\{1+\tfrac{\lambda_I}{\mu_I}\})^{-1}[\epsilon_{\mathrm{r}}^{\mathrm{S}}(5+3\tfrac{\lambda_I}{\mu_I}) + \epsilon_{\mathrm{r}}^{\mathrm{C}}(11+9\tfrac{\lambda_I}{\mu_I})](1-\cos 2\vartheta).$$

In order to obtain the displacement $\tilde{u}_{\mathrm{P}}^{(4)}$, the relative volume change is computed with the constitutive law for the pressure, yielding

$$\tilde{e}_{\mathrm{v}}^{\mathrm{S},(4)} = -3\tilde{u}_{\mathrm{P}}^{(4)} - \tfrac{3}{4}(3\epsilon_{\mathrm{r}}^{\mathrm{C}} + \epsilon_{\mathrm{r}}^{\mathrm{S}}) - \tfrac{\epsilon_{\mathrm{r}}^{\mathrm{C}} + \epsilon_{\mathrm{r}}^{\mathrm{S}}}{2(1+\frac{\lambda_I}{\mu_I})}.$$

With this result and the pressure-related factor γ, the displacement $\tilde{u}_{\mathrm{P}}^{(4)}$ follows as

$$\tilde{u}_{\mathrm{P}}^{(4)} = -\frac{1}{4}(3\epsilon_{\mathrm{r}}^{\mathrm{C}} + \epsilon_{\mathrm{r}}^{\mathrm{S}}) - \frac{1}{6}\frac{\epsilon_{\mathrm{r}}^{\mathrm{C}} + \epsilon_{\mathrm{r}}^{\mathrm{S}}}{1+\frac{\lambda_I}{\mu_I}} - \frac{1}{3}\frac{\epsilon_{\mathrm{r}}^{\mathrm{C}} + \epsilon_{\mathrm{r}}^{\mathrm{S}}}{4+3\gamma+4\frac{\lambda_I}{\mu_I}}.$$

This result is strictly negative, and hence, this force result yields an oblate deformation figure.

Computation with $\boldsymbol{f}_I^{(5)}$, where the force functions read

$$f_r^{(5)} = -(2\epsilon_{\mathrm{r}}^{\mathrm{C}}\epsilon_{\mathrm{r}}^{\mathrm{S}} - \epsilon_{\mathrm{r}}^{\mathrm{C}} - \epsilon_{\mathrm{r}}^{\mathrm{S}})\cos^2\vartheta, \quad f_\vartheta^{(5)} = 0.$$

The polar displacement follows as

$$\tilde{u}_\vartheta^{(5)}5 = \tfrac{1}{8}(2\epsilon_{\mathrm{r}}^{\mathrm{C}}\epsilon_{\mathrm{r}}^{\mathrm{S}} - \epsilon_{\mathrm{r}}^{\mathrm{C}} - \epsilon_{\mathrm{r}}^{\mathrm{S}})\sin 2\vartheta,$$

and the radial displacement in terms of $\tilde{u}_{\mathrm{P}}^{(5)}$ reads:

$$\tilde{u}_r^{(5)} = \tilde{u}_{\mathrm{P}}^{(5)} + \frac{5 + 3\frac{\lambda_I}{\mu_I}}{16(1 + \frac{\lambda_I}{\mu_I})}[2\epsilon_{\mathrm{r}}^{\mathrm{C}}\epsilon_{\mathrm{r}}^{\mathrm{S}} - \epsilon_{\mathrm{r}}^{\mathrm{C}} - \epsilon_{\mathrm{r}}^{\mathrm{S}}](1 - \cos 2\vartheta).$$

The scaled relative volume change is obtained as

$$\tilde{e}_{\mathrm{v}}^{\mathrm{S},(5)} = -3\tilde{u}_{\mathrm{P}}^{(5)} - \frac{1}{4}\frac{5 + 3\frac{\lambda_I}{\mu_I}}{1 + \frac{\lambda_I}{\mu_I}}(2\epsilon_{\mathrm{r}}^{\mathrm{C}}\epsilon_{\mathrm{r}}^{\mathrm{S}} - \epsilon_{\mathrm{r}}^{\mathrm{C}} - \epsilon_{\mathrm{r}}^{\mathrm{S}}),$$

and the pole displacement subsequently reads

$$\tilde{u}_{\mathrm{P}}^{(5)} = -(2\epsilon_{\mathrm{r}}^{\mathrm{C}}\epsilon_{\mathrm{r}}^{\mathrm{S}} - \epsilon_{\mathrm{r}}^{\mathrm{C}} - \epsilon_{\mathrm{r}}^{\mathrm{S}})\Big(\tfrac{1}{4} + \tfrac{1}{6}\frac{1}{1+\frac{\lambda_I}{\mu_I}} + \tfrac{1}{3}\frac{1}{4+3\gamma+4\frac{\lambda_I}{\mu_I}}\Big).$$

This force results also in an oblate deformation.

Comment on the parameters. The parameters γ, λ_I, and μ_I are unknown. However, it is reasonable to assume that the scales of λ_I and μ_I are equal. Hence, $\lambda_I/\mu_I \approx 1$ should be a good approximation. The effect of the parameter γ which is related to the compressibility of the system can also be analyzed. This parameter only influences the constant part of the radial displacements, *i.e.*, it does not control the qualitative deformation figure. From the solutions for the displacements of the poles, $\tilde{u}_{\mathrm{p}}^{(4)}$ and $\tilde{u}_{\mathrm{p}}^{(5)}$, it can be seen that the magnitudes of the displacements do not change significantly with the parameter $\gamma \in [0, \infty[$.

7.4 Comparison to experiment and discussion

For the static setting analyzed here, the authors in [38] conducted experiments. Their results are depicted in Fig. 14c. In the figure, it can be seen that for increasing electric field strength, the drop deforms as an oblate spheroid.

In Fig. 13, the theoretical surface force predictions of the models are qualitatively shown. Both $\boldsymbol{f}_I^{(4)}$ and $\boldsymbol{f}_I^{(5)}$ clearly suggest that the drop should deform to an oblate form. This can be observed in the experimental photographs in Fig. 14c as well. Intuitively, the surface force $\boldsymbol{f}_I^{(4)}$ may result in the correct deformation figure. The force $\boldsymbol{f}_I^5$ may cause "buckled" poles, deviating from a spheroid form. This can be observed in the deformation figure in Fig. 14. The two distinct force results both yield oblate deformation figures. However, the magnitudes of the displacements as well as the qualitative deformation figure differ. The models with the force $\boldsymbol{f}_I^{(4)}$ yield a smooth deformation figure depicted in Fig. 14a which is in good agreement with the experimental results in Fig. 14c. The deformation figure due to the models with the force $\boldsymbol{f}_I^{(5)}$ possesses a different curvature near the poles. Hence, the deformed body is not an oblate spheroid. However, this form is not observable in the experimental photographs. Therefore, it is reasonable to conclude that the models with force $\boldsymbol{f}_I^{(5)}$ yield unphysical results, *i.e.*, the asymmetric MINKOWSKI and the EINSTEIN–LAUB models are unlikely.

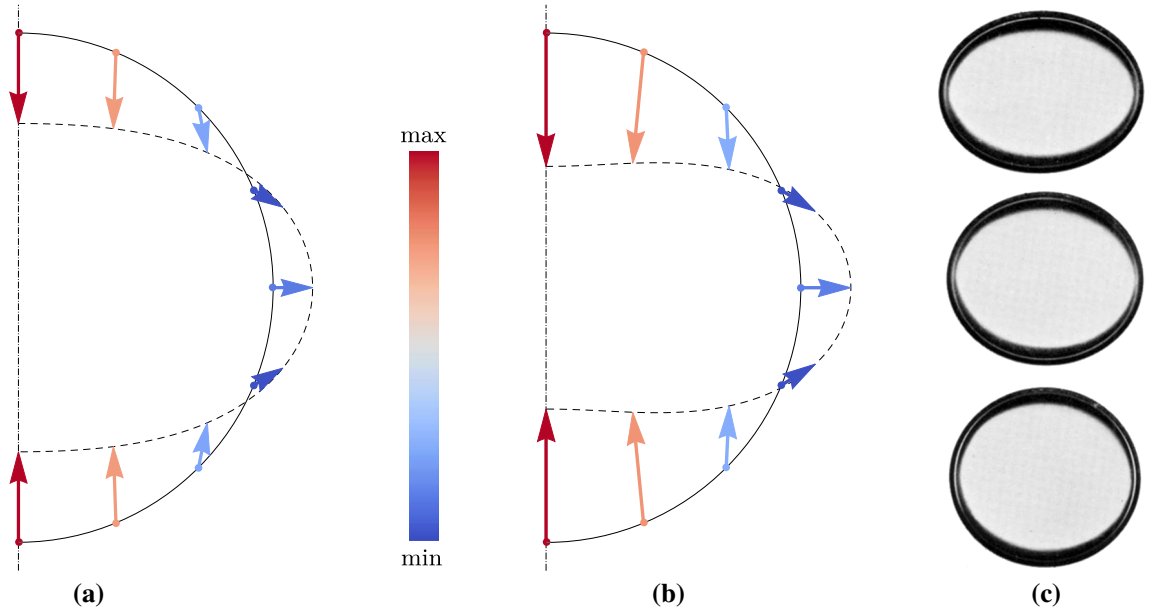

Fig. 14 Deformation figures of the oil droplet. The two solutions of the surface displacement are qualitatively shown in **a** and **b**, where the parameters $\epsilon_{\mathrm{r}}^{\mathrm{S}} = 2.8, \epsilon_{\mathrm{r}}^{\mathrm{C}} = 6.3, \gamma = 1$ and $\lambda_I/\mu_I = 1$ are used. Note that for visualization a scaling of the displacements is applied. Experimental photographs taken from [38, Fig. 7] are shown in (c). The electric field is directed vertically in all images. In **c**, the electric field strength is increased from the lowest to the highest photograph. **a** Surface displacement $\boldsymbol{u}_I^{(4)}$. **b** Surface displacement $\boldsymbol{u}_I^{(5)}$. **c** Static case of [38, Fig. 7]

8 Conclusion

In this paper, the coupling of continuum mechanics and electromagnetism was investigated. The principal question of this work is: "Does an electromagnetic force model exist, which yields correct predictions for arbitrary matter and arbitrary (dynamical) situations?" As examples a few selected electromagnetic force models were analyzed in this work. Using these, three coupled problems of mechanics and electromagnetism were investigated, *viz.*

1. the total force between two magnets,
2. magnetostriction effects of a spherical magnet, and
3. deformation of a silicone oil drop in castor oil.

In all three analyzed problems, the total force is equal for *all* considered models. In the latter two problems of local effects, this force is zero. In the problem with the two magnets, the force was computed analytically and compared with experimental findings. It was shown that the analytical findings are in good agreement with the measured force. Overall, this leads one to suspect that the total force of a body is correctly predicted with most (perhaps all) force models that are based on a balance of electromagnetic momentum.

In the problem of magnetostriction, deformations were analytically computed for the considered force models. Overall, three different deformations were obtained using the method of HIRAMATSU and OKA. As the resulting displacement amplitudes are on the nanometer scale, high-precision (laser) measurement instruments are needed to draw conclusions on the applicability of the force models. By considering a modified problem of a linear-magnetic sphere in an external field, the displacement amplitudes can be increased. This way, force model restrictions can be found from a coupled elastic and magnetic problem.

In the problem of a silicone oil drop in castor oil, an electric field causes deformations. They can be large, depending on the applied field strength. In order to make a theoretical model-dependent prediction of the surface displacements, the surface stress was modeled. The resulting differential equations were solved analytically and the deformations compared to experimental photographs. It can be concluded that the considered asymmetric MINKOWSKI and EINSTEIN–LAUB models do not reproduce the findings of this experiment. Hence, these models are not applicable in arbitrary situations.

In summary, the presented problems and experiments motivate to conceive and conduct further experiments. The few problems shown here merely scratch the surface of the problem to find a "correct" electromagnetic

force model. By varying the used materials, electromagnetic loadings, and the time dependency, it is reasonable to assume that further restrictions w.r.t. force models can be found. The last problem with the oil droplet further suggests that for fluids with electromagnetic dependencies, any general flow prediction may significantly depend on the used force model. Perhaps such (dynamical) experiments with fluids are preferable to investigations with solids. Hopefully, a force model can be found that agrees with any conducted experiment.

Acknowledgements The authors wish to thank Mr. Arion Juritza for his valuable assistance in the conduction of the axial force measurements.

Appendix A: MAXWELL's equations

In this section, a brief overview of MAXWELL's equations is given. This presentation is an extension of that given in [30]. In problems of continuum physics, steep gradients of fields may occur at the boundary of a body, (say). These are modeled by so-called singular surfaces at which the fields are modeled as discontinuous functions. These surfaces are often referred to as *interfaces* and points on them as *singular*. In these points, the differential equations of the surrounding (continuous) bulk do not apply. This also holds in the theory of electromagnetism, *i.e.*, MAXWELL's regular equations do not hold everywhere. The governing equations can be derived from balance equations in a rational manner, as described in [39]. In a domain containing a singular surface, the balances of electric charge and magnetic flux are analyzed by virtue of generalized integral and flux theorems. Limit processes yield equations for singular points that are particularly helpful in formulating boundary and transition conditions.

The results of this approach are compiled in Table 2. Interface densities are marked by the index I. The symbol $w_\perp$ denotes the normal component of the interface velocity, *i.e.*, $\boldsymbol{n}\cdot\boldsymbol{w}$. Double brackets denote the jump operator, which is defined as follows. An interface I dissects a domain in two regions, Ω_- and Ω_+. Let χ be a continuous field in the domains $\Omega_\pm$. The jump of this field is then

$$[\![\chi(\boldsymbol{x}_I,t)]\!] := \chi_+(\boldsymbol{x}_I,t) - \chi_-(\boldsymbol{x}_I,t), \quad \chi_\pm(\boldsymbol{x}_I,t) := \lim_{\boldsymbol{x}_\pm\to\boldsymbol{x}_I}\chi(\boldsymbol{x}_\pm), \quad \boldsymbol{x}_\pm\in\Omega_\pm, \quad \boldsymbol{x}_I\in I. \tag{A.1a}$$

Of course, there is some arbitrariness which side is referred to as $+$ or $-$. However, this causes no problems when applying the chosen definition everywhere. In this paper, we employ the convention that $-$ and $+$ refer to the inside and outside of a considered domain, respectively. The direction of the normal vector is defined at a point from the $-$ into the $+$ domain. Another interface operator is the mean value, given by

$$\langle\chi(\boldsymbol{x}_I,t)\rangle := \tfrac{1}{2}(\chi_+(\boldsymbol{x}_I,t)+\chi_-(\boldsymbol{x}_I,t)), \quad \chi_\pm(\boldsymbol{x}_I,t) := \lim_{\boldsymbol{x}_\pm\to\boldsymbol{x}_I}\chi(\boldsymbol{x}_\pm), \quad \boldsymbol{x}_\pm\in\Omega_\pm, \quad \boldsymbol{x}_I\in I. \tag{A.1b}$$

In the context of continuum physics, the symbols in the equations of Table 2 are identified in this paper as follows. The fields $\boldsymbol{E}$ and $\boldsymbol{B}$ are referred to as the electric field and the magnetic flux density, respectively. They

Table 2 MAXWELL's equations in multiple forms

	Regular points	Singular points
FARADAY's law of induction	$\frac{\partial\boldsymbol{B}}{\partial t}+\nabla\times\boldsymbol{E}=\boldsymbol{0}$	$-[\![\boldsymbol{B}]\!]w_\perp+\boldsymbol{n}\times[\![\boldsymbol{E}]\!]=\boldsymbol{0}$
GAUSS' law for magnetism	$\nabla\cdot\boldsymbol{B}=0$	$\boldsymbol{n}\cdot[\![\boldsymbol{B}]\!]=0$
AMPÈRE's law	$\frac{\partial\mathfrak{D}}{\partial t}-\nabla\times\mathfrak{H}=-\boldsymbol{J}^{\mathrm{f}}$	$-[\![\mathfrak{D}]\!]w_\perp-\boldsymbol{n}\times[\![\mathfrak{H}]\!]=-\boldsymbol{j}_I^{\mathrm{f}}$
GAUSS' law	$\nabla\cdot\mathfrak{D}=q^{\mathrm{f}}$	$\boldsymbol{n}\cdot[\![\mathfrak{D}]\!]=q_I^{\mathrm{f}}$
Total electric current	$\frac{\partial\boldsymbol{D}}{\partial t}-\nabla\times\boldsymbol{H}=-\boldsymbol{J}$	$-[\![\boldsymbol{D}]\!]w_\perp-\boldsymbol{n}\times[\![\boldsymbol{H}]\!]=-\boldsymbol{J}_I$
Total electric charge	$\nabla\cdot\boldsymbol{D}=q$	$\boldsymbol{n}\cdot[\![\boldsymbol{D}]\!]=q_I$
Non-free electric current	$-\frac{\partial\boldsymbol{P}}{\partial t}-\nabla\times\boldsymbol{M}=-\boldsymbol{J}^{\mathrm{r}}$	$[\![\boldsymbol{P}]\!]w_\perp-\boldsymbol{n}\times[\![\boldsymbol{M}]\!]=-\boldsymbol{J}_I^{\mathrm{r}}$
Non-free electric charge	$-\nabla\cdot\boldsymbol{P}=q^{\mathrm{r}}$	$-\boldsymbol{n}\cdot[\![\boldsymbol{P}]\!]=q_I^{\mathrm{r}}$

are not independent of each other. Rather, they are parts of a four-dimensional space–time tensor. The same holds for the fields ($\boldsymbol{D}$, $\boldsymbol{H}$) and ($\mathfrak{D}$, $\mathfrak{H}$). In continuum electromagnetism, the fields $\boldsymbol{D}$ and $\mathfrak{D}$ are referred to as charge potentials w.r.t. total and free charge, respectively. Analogously, $\boldsymbol{H}$ and $\mathfrak{H}$ are the current potentials w.r.t. total and free electric current. Their definitions are based on the balances of total and free electric current. Further, q and q^{f} are the total and free charge density, $\boldsymbol{J}$ and $\boldsymbol{J}^{\mathrm{f}}$ the total and free electric current density. If the index "f" is exchanged with "r", densities w.r.t. the balance of bound electric charge will result. This balance gives rise to potential fields $\boldsymbol{P}$ and $\boldsymbol{M}$, which are properly called bound charge potential and bound current potential, respectively. In this work, they are referred to by their more common names, *i.e.*, polarization and (MINKOWSKI) magnetization. The presentation of MAXWELL's equations and the fields contained within follows [18]. It can be noted that there are other formulations of MAXWELL's equations in the literature, *e.g.*, the CHU formulation. A thorough review of various formulations is given in [16].

Since the balances of total, free, and bound electric charge are not independent of each other, the following relations hold everywhere:

$$q = q^{\mathrm{f}} + q^{\mathrm{r}}, \quad \boldsymbol{J} = \boldsymbol{J}^{\mathrm{f}} + \boldsymbol{J}^{\mathrm{r}}, \quad \boldsymbol{H} = \mathfrak{H} + \boldsymbol{M}, \quad \boldsymbol{D} = \mathfrak{D} - \boldsymbol{P}, \quad \boldsymbol{H} = \tfrac{1}{\mu_0}\boldsymbol{B}, \quad \boldsymbol{D} = \varepsilon_0 \boldsymbol{E}. \tag{A.2a}$$

The two last formulæ are called MAXWELL–LORENTZ aether relations. They connect the potentials of total electric charge and of total electric current with the fields $\boldsymbol{E}$ and $\boldsymbol{B}$, inside and outside of matter. It can often be beneficial to decompose the free electric current density into a diffusive ($\boldsymbol{j}^{\mathrm{f}}$) and a non-diffusive part ($q^{\mathrm{f}}\boldsymbol{v}$), that can loosely be referred to as non-convective and convective electric current densities, respectively:

$$\boldsymbol{J}^{\mathrm{f}} = q^{\mathrm{f}}\boldsymbol{v} + \boldsymbol{j}^{\mathrm{f}}, \quad \boldsymbol{J}^{\mathrm{f}}_{I} = q^{\mathrm{f}}_{I}\boldsymbol{v}_{I} + \boldsymbol{j}^{\mathrm{f}}_{I}. \tag{A.2b}$$

Here, $\boldsymbol{v}$ denotes the barycentric velocity of a medium. A theory of mixtures in context of electromagnetism is detailed in [13]. For a review of continuum electromagnetism see [18].

Appendix B: Balance of linear momentum for regular and singular points

In this section, the local balance equations of linear momentum in regular and singular points are briefly stated. In the derivation, a classical EULER–CAUCHY continuum is assumed. In regular points, the balance reads

$$\rho\boldsymbol{A} - \boldsymbol{\sigma}\cdot\nabla = \rho\boldsymbol{F} + \boldsymbol{f}^{(\mathrm{EM})}. \tag{B.1}$$

Herein, the body forces are decomposed into the classical mass-proportional density, $\rho\boldsymbol{F}$, and an electromagnetic source $\boldsymbol{f}^{(\mathrm{EM})}$. In this equation, $\boldsymbol{\sigma}$ denotes the pure *mechanical* stress tensor. By introducing the surface nabla operator via the projection

$$\nabla_I := \mathbf{1}_I \cdot \nabla \quad \text{where} \quad \mathbf{1}_I = \mathbf{1} - \boldsymbol{n}\otimes\boldsymbol{n},$$

the balance of linear momentum in singular points reads

$$\rho_I\boldsymbol{a}_I - \boldsymbol{\sigma}_I\cdot\nabla_I = -[\![\rho(\boldsymbol{v}-\boldsymbol{v}_I)\otimes(\boldsymbol{v}-\boldsymbol{w}) - \boldsymbol{\sigma}]\!]\cdot\boldsymbol{n} + \rho_I\boldsymbol{F}_I + \boldsymbol{f}^{(\mathrm{EM})}_I, \tag{B.2}$$

This equation also contains a decomposed force density w.r.t. mass and electromagnetism. The static version of this equation reduces to

$$-\boldsymbol{\sigma}_I\cdot\nabla_I = [\![\boldsymbol{\sigma}]\!]\cdot\boldsymbol{n} + \rho_I\boldsymbol{F}_I + \boldsymbol{f}^{(\mathrm{EM})}_I. \tag{B.3}$$

If the singular surface is without intrinsic structure, this equation further simplifies to

$$\mathbf{0} = [\![\boldsymbol{\sigma}]\!]\cdot\boldsymbol{n} + \boldsymbol{f}^{(\mathrm{EM})}_I. \tag{B.4}$$

As the electromagnetic surface traction is not (purely) intrinsic to the interface, it remains in the equation. This density can be related to regular field values in close proximity of the surface, depending on the force model employed. For thorough reviews of balance equations for regular and singular points, see [8,34,36].

Appendix C: Example of the form computation of electromagnetic force formulas

In this section, it is shown how the form of electromagnetic force densities can be obtained. As an example, the generalized LORENTZ force model is used. For the analysis, the following formulas of vector calculus identities are useful:

$$\boldsymbol{a}\times(\boldsymbol{b}\times\boldsymbol{c})=\boldsymbol{b}(\boldsymbol{a}\cdot\boldsymbol{c})-\boldsymbol{c}(\boldsymbol{a}\cdot\boldsymbol{b}),\qquad (\nabla\times\boldsymbol{a})\times\boldsymbol{b}=\boldsymbol{b}\cdot(\nabla\otimes\boldsymbol{a})-(\nabla\otimes\boldsymbol{a})\cdot\boldsymbol{b},$$
$$\nabla\cdot(\boldsymbol{a}\otimes\boldsymbol{b})=(\nabla\cdot\boldsymbol{a})\boldsymbol{b}+\boldsymbol{a}\cdot(\nabla\otimes\boldsymbol{b}),\qquad (\nabla\otimes\boldsymbol{a})\cdot\boldsymbol{a}=\nabla\tfrac{1}{2}\|\boldsymbol{a}\|^2=\nabla\cdot\tfrac{1}{2}\|\boldsymbol{a}\|^2\mathbf{1},$$
$$(\nabla\times\boldsymbol{a})\times\boldsymbol{b}=\nabla\cdot(\boldsymbol{b}\otimes\boldsymbol{a})-(\nabla\cdot\boldsymbol{b})\boldsymbol{a}-(\nabla\otimes\boldsymbol{a})\cdot\boldsymbol{b},\qquad [\![ab]\!]=[\![a]\!]\langle b\rangle+\langle a\rangle[\![b]\!].$$

Here, $\boldsymbol{a}$, $\boldsymbol{b}$, $\boldsymbol{c}$ are smooth vector fields and a, b are scalar fields.

Let us assume that the generalized LORENTZ force model is defined by a momentum density and stress tensor

$$\boldsymbol{g}^{\mathrm{L}}=\boldsymbol{D}\times\boldsymbol{B},\quad \boldsymbol{\sigma}^{\mathrm{L}}=-\tfrac{1}{2}(\epsilon_0\boldsymbol{E}\cdot\boldsymbol{E}+\tfrac{1}{\mu_0}\boldsymbol{B}\cdot\boldsymbol{B})\mathbf{1}+\epsilon_0\boldsymbol{E}\otimes\boldsymbol{E}+\tfrac{1}{\mu_0}\boldsymbol{B}\otimes\boldsymbol{B},$$

so that

$$\frac{\partial}{\partial t}(\boldsymbol{g}^{\mathrm{L}})-\nabla\cdot\boldsymbol{\sigma}^{\mathrm{L}}=-\boldsymbol{f}^{\mathrm{L}}.$$

To obtain $\boldsymbol{f}^{\mathrm{L}}$, one can start by examining the time derivative of the momentum density:

$$\begin{aligned}
\frac{\partial(\boldsymbol{D}\times\boldsymbol{B})}{\partial t}&=\frac{\partial\boldsymbol{D}}{\partial t}\times\boldsymbol{B}+\boldsymbol{D}\times\frac{\partial\boldsymbol{B}}{\partial t}\\
&=(\nabla\times\boldsymbol{H}-\boldsymbol{J})\times\boldsymbol{B}+\boldsymbol{D}\times(-\nabla\times\boldsymbol{E})=(\nabla\times\boldsymbol{H})\times\boldsymbol{B}+(\nabla\times\boldsymbol{E})\times\boldsymbol{D}-\boldsymbol{J}\times\boldsymbol{B}\\
&=\boldsymbol{B}\cdot(\nabla\otimes\boldsymbol{H})-(\nabla\otimes\boldsymbol{H})\cdot\boldsymbol{B}+\boldsymbol{D}\cdot(\nabla\otimes\boldsymbol{E})-(\nabla\otimes\boldsymbol{E})\cdot\boldsymbol{D}-\boldsymbol{J}\times\boldsymbol{B}\\
&=\tfrac{1}{\mu_0}\boldsymbol{B}\cdot(\nabla\otimes\boldsymbol{B})-\tfrac{1}{\mu_0}(\nabla\otimes\boldsymbol{B})\cdot\boldsymbol{B}+\epsilon_0\boldsymbol{E}\cdot(\nabla\otimes\boldsymbol{E})-\epsilon_0(\nabla\otimes\boldsymbol{E})\cdot\boldsymbol{E}-\boldsymbol{J}\times\boldsymbol{B}\\
&=\tfrac{1}{\mu_0}\nabla\cdot(\boldsymbol{B}\otimes\boldsymbol{B})-\tfrac{1}{\mu_0}(\nabla\cdot\boldsymbol{B})\boldsymbol{B}-\tfrac{1}{\mu_0}\nabla\cdot(\tfrac{1}{2}\boldsymbol{B}\cdot\boldsymbol{B})\mathbf{1}+\epsilon_0\nabla\cdot(\boldsymbol{E}\otimes\boldsymbol{E})-\\
&\qquad-(\nabla\cdot\epsilon_0\boldsymbol{E})\boldsymbol{E}-\epsilon_0\nabla\cdot(\tfrac{1}{2}\boldsymbol{E}\cdot\boldsymbol{E})\mathbf{1}-\boldsymbol{J}\times\boldsymbol{B}\\
&=\nabla\cdot[-\tfrac{1}{2}(\epsilon_0\boldsymbol{E}\cdot\boldsymbol{E}+\tfrac{1}{\mu_0}\boldsymbol{B}\cdot\boldsymbol{B})\mathbf{1}+\epsilon_0\boldsymbol{E}\otimes\boldsymbol{E}+\tfrac{1}{\mu_0}\boldsymbol{B}\otimes\boldsymbol{B}]-q\boldsymbol{E}-\boldsymbol{J}\times\boldsymbol{B}.
\end{aligned}$$

In these computations, MAXWELL's equations and some of the above identities of vector calculus were used. As for this force model, the stress tensor is specified, the force density is uniquely defined as $\boldsymbol{f}^{\mathrm{L}}=q\boldsymbol{E}+\boldsymbol{J}\times\boldsymbol{B}$. If only the momentum density is fixed, then there are infinitely many options to define the electromagnetic stress and force.

The surface force $\boldsymbol{f}_I^{\mathrm{L}}=\boldsymbol{n}\cdot[\![\boldsymbol{w}\otimes\boldsymbol{g}^{\mathrm{L}}+\boldsymbol{\sigma}^{\mathrm{L}}]\!]$ is computed next, using the singular forms of MAXWELL's equations and the product rule of jumps shown above. Starting with

$$\boldsymbol{f}_I^{\mathrm{L}}=\boldsymbol{n}\cdot[\![\boldsymbol{w}\otimes(\boldsymbol{D}\times\boldsymbol{B})-\tfrac{1}{2}(\epsilon_0\boldsymbol{E}\cdot\boldsymbol{E}+\tfrac{1}{\mu_0}\boldsymbol{B}\cdot\boldsymbol{B})\mathbf{1}+\epsilon_0\boldsymbol{E}\otimes\boldsymbol{E}+\tfrac{1}{\mu_0}\boldsymbol{B}\otimes\boldsymbol{B}]\!],$$

it is convenient to regard the contained terms individually. The first becomes

$$\begin{aligned}
\boldsymbol{n}\cdot[\![\boldsymbol{w}\otimes(\boldsymbol{D}\times\boldsymbol{B})]\!]&=w_\perp\epsilon_0[\![\boldsymbol{E}\times\boldsymbol{B}]\!]=w_\perp\epsilon_0[\![\boldsymbol{E}]\!]\times\langle\boldsymbol{B}\rangle+\epsilon_0\langle\boldsymbol{E}\rangle\times w_\perp[\![\boldsymbol{B}]\!]\\
&=(\boldsymbol{J}_I-\boldsymbol{n}\times[\![\boldsymbol{H}]\!])\times\langle\boldsymbol{B}\rangle+\epsilon_0\langle\boldsymbol{E}\rangle\times(\boldsymbol{n}\times[\![\boldsymbol{E}]\!])\\
&=\tfrac{1}{\mu_0}\langle\boldsymbol{B}\rangle\times(\boldsymbol{n}\times[\![\boldsymbol{B}]\!])+\epsilon_0\langle\boldsymbol{E}\rangle\times(\boldsymbol{n}\times[\![\boldsymbol{E}]\!])+\boldsymbol{J}_I\times\langle\boldsymbol{B}\rangle\\
&=\tfrac{1}{\mu_0}\boldsymbol{n}\langle\boldsymbol{B}\rangle\cdot[\![\boldsymbol{B}]\!]-\tfrac{1}{\mu_0}[\![\boldsymbol{B}]\!]\langle\boldsymbol{B}\rangle\cdot\boldsymbol{n}+\epsilon_0\boldsymbol{n}\langle\boldsymbol{E}\rangle\cdot[\![\boldsymbol{E}]\!]-\epsilon_0[\![\boldsymbol{E}]\!]\langle\boldsymbol{E}\rangle\cdot\boldsymbol{n}+\boldsymbol{J}_I\times\langle\boldsymbol{B}\rangle.
\end{aligned}$$

The second term is manipulated to read

$$\boldsymbol{n}\cdot[\![-\tfrac{1}{2}(\epsilon_0\boldsymbol{E}\cdot\boldsymbol{E}+\tfrac{1}{\mu_0}\boldsymbol{B}\cdot\boldsymbol{B})\mathbf{1}]\!]=-\tfrac{1}{2}\boldsymbol{n}[\![(\epsilon_0\boldsymbol{E}\cdot\boldsymbol{E}+\tfrac{1}{\mu_0}\boldsymbol{B}\cdot\boldsymbol{B})]\!]=-\epsilon_0\boldsymbol{n}\langle\boldsymbol{E}\rangle\cdot[\![\boldsymbol{E}]\!]-\tfrac{1}{\mu_0}\boldsymbol{n}\langle\boldsymbol{B}\rangle\cdot[\![\boldsymbol{B}]\!],$$

and the last term becomes

$$\begin{aligned}
\boldsymbol{n}\cdot[\![\epsilon_0\boldsymbol{E}\otimes\boldsymbol{E}+\tfrac{1}{\mu_0}\boldsymbol{B}\otimes\boldsymbol{B}]\!]&=\epsilon_0\boldsymbol{n}\cdot\langle\boldsymbol{E}\rangle[\![\boldsymbol{E}]\!]+\epsilon_0\boldsymbol{n}\cdot[\![\boldsymbol{E}]\!]\langle\boldsymbol{E}\rangle+\tfrac{1}{\mu_0}\boldsymbol{n}\cdot\langle\boldsymbol{B}\rangle[\![\boldsymbol{B}]\!]+\tfrac{1}{\mu_0}\boldsymbol{n}\cdot[\![\boldsymbol{B}]\!]\langle\boldsymbol{B}\rangle\\
&=\epsilon_0\boldsymbol{n}\cdot\langle\boldsymbol{E}\rangle[\![\boldsymbol{E}]\!]+q_I\langle\boldsymbol{E}\rangle+\tfrac{1}{\mu_0}\boldsymbol{n}\cdot\langle\boldsymbol{B}\rangle[\![\boldsymbol{B}]\!].
\end{aligned}$$

Summing the three terms shows that many contributions cancel out, and there remains

$$\boldsymbol{f}_I^{\mathrm{L}}=q_I\langle\boldsymbol{E}\rangle+\boldsymbol{J}_I\times\langle\boldsymbol{B}\rangle.$$

References

1. Abraham, M.: Zur Elektrodynamik bewegter Körper. Rendiconti del Circolo Matematico di Palermo (1884–1940) **28**(1), 1–28 (1909)
2. Abramowitz, M., Stegun, I.A. (eds.): Handbook of Mathematical Functions with Formulas, Graphs, and Mathematical Tables, vol. 9. Dover (1972)
3. Barnett, S.M.: Resolution of the Abraham–Minkowski dilemma. Phys. Rev. Lett. **104**(7), 070401 (2010)
4. Barnett, S.M., Loudon, R.: On the electromagnetic force on a dielectric medium. J. Phys. B At. Mol. Opt. Phys. **39**(15), 671–684 (2006)
5. Bethune-Waddell, M., Chau, K.J.: Simulations of radiation pressure experiments narrow down the energy and momentum of light in matter. Rep. Prog. Phys. **78**(12), 122401 (2015)
6. Chu, L.J., Haus, H.A., Penfield, P.: The force density in polarizable and magnetizable fluids. Proc. IEEE **54**(7), 920–935 (1966)
7. Datsyuk, V.V., Pavlyniuk, O.R.: Maxwell stress on a small dielectric sphere in a dielectric. Phys. Rev. A **91**(2), 023826 (2015)
8. Dziubek, A.: Equations for two-phase flows: a primer. ArXiv e-prints (2011)
9. Einstein, A., Laub, J.: Über die im elektromagnetischen Felde auf ruhende Körper ausgeübten ponderomotorischen Kräfte. Ann. Phys. **331**(8), 541–550 (1908)
10. Fitzpatrick, R.: Classical Electromagnetism. The University of Texas at Austin, Austin (2006)
11. Gradshteyn, I.S., Ryzhik, I.M.: Table of integrals, series, and products, 7th edn. Academic Press, Cambridge (2007)
12. Griffiths, D.J.: Resource letter em-1: electromagnetic momentum. Am. J. Phys. **80**(1), 7–18 (2012)
13. Guhlke, C.: Theorie der elektrochemischen Grenzfläche. Ph.D. thesis, Technische Universität Berlin (2015)
14. Hiramatsu, Y., Oka, Y.: Determination of the tensile strength of rock by a compression test of an irregular test piece. Int. J. Rock Mech. Min. Sci. Geomech. Abstr. **3**(2), 89–90 (1966)
15. Hutter, K.: On thermodynamics and thermostatics of viscous thermoelastic solids in the electromagnetic fields. A Lagrangian formulation. Arch. Ration. Mech. Anal. **58**, 339–368 (1975)
16. Hutter, K., Ven, A.A.F., Ursescu, A.: Electromagnetic Field Matter Interactions in Thermoelastic Solids and Viscous Fluids. Springer, Berlin (2006)
17. Jackson, J.D.: Classical Electrodynamics, 2nd edn. Wiley, Hoboken (1975)
18. Kovetz, A.: Electromagnetic Theory. Oxford University Press, Oxford (2000)
19. Liebold, C., Müller, W.H.: Are microcontinuum field theories of elasticity amenable to experiments? A review of some recent results. In: Differential Geometry and Continuum Mechanics, pp. 255–278. Springer Nature (2015)
20. magnets4you GmbH: Bar magnet STM-20x34-N (2016). https://www.magnet-shop.net/media/pdf/de/1c/a4/Datenblatt_STM-20x34-N.pdf
21. Mahdy, M.C.M.: It should be Einstein-Laub equations inside matter. arXiv preprint arXiv:1211.0155 (2012)
22. Mansuripur, M.: Resolution of the Abraham–Minkowski controversy. Opt. Commun. **283**(10), 1997–2005 (2010)
23. Mansuripur, M.: Electromagnetic force and torque in Lorentz and Einstein-Laub formulations. In: SPIE NanoScience + Engineering. International Society for Optics and Photonics (2014)
24. Minkowski, H.: Die Grundgleichungen für die elektromagnetischen Vorgänge in bewegten Körpern. Math. Ann. **68**(4), 472–525 (1910)
25. MTS Systems Corporation, Eden Prairie, Minnesota 55344-2290 USA: Tytron^{TM} 250 Microforce Load Unit (2002). http://www.mts.com/cs/groups/public/documents/library/mts_004918.pdf
26. Müller, I.: Thermodynamics, Interaction of Mechanics and Mathematics Series. Pitman, Trowbridge (1985)
27. Müller, W.H.: An Expedition to Continuum Theory. Solid mechanics and its applications series. Springer, Berlin (2014)
28. Obukhov, Y.N.: Electromagnetic energy and momentum in moving media. Ann. Phys. **17**(9–10), 830–851 (2008)
29. Raikher, Y.L., Stolbov, O.V.: Deformation of an ellipsoidal ferrogel sample in a uniform magnetic field. J. Appl. Mech. Tech. Phys. **46**(3), 434–443 (2005)
30. Reich, F.A., Rickert, W., Stahn, O., Müller, W.H.: Magnetostriction of a sphere: stress development during magnetization and residual stresses due to the remanent field. Contin. Mech. Thermodyn. **29**(2), 535–557 (2016)
31. Reich, F.A., Stahn, O., Müller, W.H.: The magnetic field of a permanent hollow cylindrical magnet. Contin. Mech. Thermodyn. **28**(5), 1435–1444 (2016)
32. Shah, D.O.: Improved Oil Recovery by Surfactant and Polymer Flooding. Academic Press, Cambridge (1977)
33. Shevchenko, A., Kaivola, M.: Electromagnetic force density and energy-momentum tensor in an arbitrary continuous medium. J. Phys. B At. Mol. Opt. Phys. **44**(17), 175401 (2011)
34. Slattery, J.C., Sagis, L., Oh, E.S.: Interfacial Transport Phenomena. Springer, Berlin (2007)
35. Steigmann, D.J.: On the formulation of balance laws for electromagnetic continua. Math. Mech. Solids **14**(4), 390–402 (2009)
36. Steinmann, P.: On boundary potential energies in deformational and configurational mechanics. J. Mech. Phys. Solids **56**(3), 772–800 (2008)
37. Stratton, J.A.: Electromagnetic Theory. McGraw-Hill, New York (1941)
38. Torza, S., Cox, R.G., Mason, S.G.: Electrohydrodynamic deformation and burst of liquid drops. Philos. Trans. R. Soc. A Math. Phys. Eng. Sci. **269**(1198), 295–319 (1971)
39. Truesdell, C.A., Toupin, R.: The classical field theories. In: Handbuch der Physik, Bd. III/1, pp. 226–793; appendix, pp. 794–858. Springer, Berlin (1960). With an appendix on tensor fields by J.L. Ericksen
40. Wang, C.: Comment on "resolution of the Abraham–Minkowski dilemma". arXiv preprint arXiv:1202.2575 (2012)
41. Wolfram Research, Inc.: Mathematica, 11 edn. (2016)